

This is the peer reviewed version of the following article:

Experimental analysis of pre-compressed circular cylindrical shell under axial harmonic load / Zippo, Antonio; Barbieri, Marco; Pellicano, Francesco. - In: INTERNATIONAL JOURNAL OF NON-LINEAR MECHANICS. - ISSN 0020-7462. - STAMPA. - 94:(2017), pp. 417-440. [10.1016/j.ijnonlinmec.2016.11.004]

Terms of use:

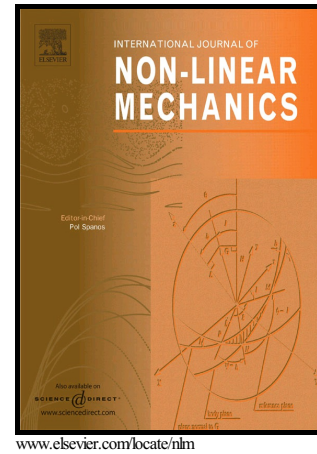
The terms and conditions for the reuse of this version of the manuscript are specified in the publishing policy. For all terms of use and more information see the publisher's website.

18/12/2025 19:33

Author's Accepted Manuscript

Experimental analysis of pre-compressed circular cylindrical shell under axial harmonic load

Antonio Zippo, Marco Barbieri, Francesco Pellicano



PII: S0020-7462(16)30320-1

DOI: <http://dx.doi.org/10.1016/j.ijnonlinmec.2016.11.004>

Reference: NLM2734

To appear in: *International Journal of Non-Linear Mechanics*

Received date: 30 June 2016

Revised date: 7 November 2016

Accepted date: 15 November 2016

Cite this article as: Antonio Zippo, Marco Barbieri and Francesco Pellicano
Experimental analysis of pre-compressed circular cylindrical shell under axial
harmonic load, *International Journal of Non-Linear Mechanics*
<http://dx.doi.org/10.1016/j.ijnonlinmec.2016.11.004>

This is a PDF file of an unedited manuscript that has been accepted for publication. As a service to our customers we are providing this early version of the manuscript. The manuscript will undergo copyediting, typesetting, and review of the resulting galley proof before it is published in its final citable form. Please note that during the production process errors may be discovered which could affect the content, and all legal disclaimers that apply to the journal pertain.

Experimental analysis of pre-compressed circular cylindrical shell under axial harmonic load

Antonio Zippo^{a,*}, Marco Barbieri^a, Francesco Pellicano^a

^a*Department of Engineering “Enzo Ferrari”, University of Modena and Reggio Emilia,
Via Pietro Vivarelli 10, 41125 Modena, Italy*

Abstract

In this paper the nonlinear dynamics of circular cylindrical shells under axial static (compressive) and periodic resonant loads have been experimentally investigated, the goal is to study the dynamic scenario and to analyze non-linear regimes. A special test rig has been developed for the experiment in order to apply a static axial load combined with a dynamic axial load. The setup allows for investigating the linear behavior under static preload by means of the usual modal testing techniques; moreover, it allows for analyzing the nonlinear response which occurs when the dynamic axial load is periodic and gives rise to complex resonances. The complex dynamics, arising when a periodic axial load excites the asymmetric (shell like) modes, are analyzed by means of amplitude frequency diagrams, waterfall spectrum diagrams, bifurcation diagrams of Poincaré maps; a deep analysis of time histories, spectra, phase portraits and Poincaré maps completes the study of the complex dynamic scenario.

Keywords: Circular cylindrical shell, experiments, non-linear dynamics, chaos

1. Introduction

There is an historical interest in studying the dynamics of shells; the first motivation is the wide presence of such elements in any field of structural

*Corresponding author

Email addresses: antonio.zippo@unimore.it (Antonio Zippo), mark@unimore.it (Marco Barbieri), francesco.pellicano@unimore.it (Francesco Pellicano)

engineering: Aerospace (wings and fuselage panels, parts of rockets and missiles, parts of space structures and satellites); Automotive (car hoods and doors, top panels, car firewall panels); Civil (vaults, marquees, tanks, tubular towers, silos, pressure vessels); Nuclear (heat exchangers, pipes and pipe clusters, cooling towers); Marine (ship panels and plates, offshore platform sub-structures).

Shells are widely used by structural engineers due to their strength-to-weight efficiency; the need of more and more efficient structures in terms of strength and weight led to a strong reduction of safety factors; one of the direct consequences of weight reduction is the increment of stability and vibration problems.

Shells usually exhibit a complicated dynamic behavior because the curvature strongly couples flexural and in-plane deformations, and the three displacement and three rotation fields simultaneously appear in each of the governing partial differential equations and boundary conditions (for thin shells rotations are dependent on the displacements, so they are not real unknowns in the governing equations). Therefore, it is clear that the axial constraints can have direct effects on predominantly radial modes. For instance, it has been shown that the natural frequencies for the circumferential modes of a simply supported circular cylindrical shell can be noticeably modified by the constraints applied in the axial direction, see e.g. Ref.[1], p. 140 Figure 2.110.

Vibrations of shells have been extensively studied for several decades, numerous shell theories take to account various effects associated with deformations or stress components. Thousands of papers can be found in the literature, mainly devoted to theoretical analyses of the linear vibration; the scientific production regarding the shell nonlinear vibrations is less wide but quite large; eventually, experimental studies on the nonlinear vibration of shells are not numerous.

The high modal density of shell structures can cause resonances and consequently high amplitude vibrations. It is well known that moderately high amplitudes of vibration in shells give rise to strong nonlinear phenomena such as: super and sub harmonic response, quasiperiodic motion, chaos. This is well documented by a large scientific literature, mostly focused on modeling and much less on experimentation. For a comprehensive literature analysis the reader is suggested to read Refs. [1–8] where very interesting reviews of the western and eastern literature can be found, as well as details regarding theories and the most representative experimental findings.

Nowadays, commercial software allows to carry out static, stability and vibration analyses; however, regarding shell dynamics, such kind of analyses are usually reliable in the linear field only. Moreover, numerical investigation are even less reliable for composite materials where the properties are strongly dependent from fibre arrangement along the geometry. Experimental studies in nonlinear dynamics play a key role and have a high relevance both to validate numerical and theoretical models and to highlight/discover specific behaviors predicted by the theoretical models, this is particularly important for new materials (composite carbon fibre, etc.) due to their intrinsic nonlinear properties and their innovative applications.

Difficulties in developing accurate models for shell structures were the motivations of a large scientific production, withal there are few experimental studies [9] about dynamic instabilities and the comparisons between theory and experiments are not yet satisfactory.

The fundamental investigation on the stability of circular cylindrical shells is due to Von Karman and Tsien [2] who analyzed the static stability (buckling) and the postcritical behavior of axially loaded shells. In this study, it was clarified that the discrepancies between forecasts of linear models and experimental results were due to the intrinsic simplifications of linear models; indeed, linear analyses are not able to predict the actual buckling phenomenon observed in experiments.

Vijayaraghavan and Evan-Iwanowski [10] analyzed, both analytically and experimentally, the parametric instabilities of a circular shell under seismic excitation. The cylinder position was vertical and the base was axially excited using a shaker. Instability regions were found analytically and compared to experimental results.

Suoza [11] proposed an analytical investigation of the dynamics of thin-walled structural systems for both the pre- and the post-buckling states. Sofiyev and Kuruoglu [12] analyzed the vibration and buckling of functionally graded (FG) orthotropic cylindrical shells under external pressures using the shear deformation shell theory (SDST); differences between the parabolic shear deformation theory (PSDT) and several higher-order shear deformation theories (HSDTs) were investigated. In 2013 Strozzi and Pellicano [13] analyzed the nonlinear vibrations of functionally graded (FGM) circular cylindrical shells.

Recently, the problem of active vibration control of shell structures has received increasing interest by many researchers. Ray and Shivakumar [14] published a paper focused on vibration control using an active constrained

layer damping (ACLD), applied to geometrically nonlinear transient vibrations of a laminated thin composite plate. Zippo et al. [15] proposed an active vibration control of a free-edge rectangular sandwich plate; the experimental setup consisted of a honeycomb panel having a carbon-fiber reinforced polymer outer skin and a polymer-paper core. Jafari et al. [16] studied nonlinear vibrations of simply supported functionally graded (FG) cylindrical shells with embedded piezoelectric layers.

The Donnell's nonlinear shallow-shell theory [17] was used by Gonçalves and Del Prado [18] to analyze the dynamic buckling of a perfect circular cylindrical shell under axial static and dynamic loads. Pellicano and Avramov [19] published a paper concerning the nonlinear dynamics of a shell carrying a top disk with base excitation. The work was mainly theoretical and only some experimental results concerning the linear dynamics were presented. The shell was modeled using the nonlinear Sanders Koiter theory [17] and a reduced order model was used. Kubenko and Kovalchuk [20] published an experimental work focused on shells made of composite materials; they pointed out the inadequateness of the linear viscous damping models; axial loads (base excitation, and free top end of the shell) as well as combined loads were considered. Dynamic instability regions were determined experimentally: a disagreement between previous theoretical models (narrower region) and experiments (wider) was found, the conjecture made by such scientists was that the disagreement was due to shells geometric imperfections. This paper summarizes some of the experimental results published on a previous book (Kubenko et al.) [4] (see e.g. page 123, Figure 2.23 gives an interpretation of the enlargement of instability boundaries).

Patel et al. [21] studied the static and dynamic instability characteristics of stiffened shell panels subjected to uniform in-plane harmonic edge loading; they used the method of Hill's infinite determinant to analyze dynamic instability regions.

Nonlinear free vibration analysis of prestressed circular cylindrical shells placed on Winkler/Pasternak foundation was investigated in Ref. [22]. The nonlinear Sanders-Koiter shell theory and the classical nonlinear Love's thin shell theory were also applied in some specific cases to check the coherence of the results. Perturbation methods were used to find the relationship between vibration amplitude and frequency in nonlinear state.

In 2012 Pellicano [23] presented an early experimental study on circular cylindrical shells under base excitation, more recent experimental results are presented in [24]. A theoretical model is developed to reproduce the

experimental evidence and provide an explanation of the complex dynamics observed experimentally [25–27].

In the present paper, a setup for testing a circular cylindrical shell under static axial (compressive) load is described. The linear dynamics of the shell under preload is investigated by means of impact testing, while the non-linear behaviors under combined static and dynamic axial loads are extensively investigated.

2. Setup and test description

This section provides information about the experimental setup developed to test thin shell structures under constant compressive load plus a periodic axial load. In Figure 1a a schematic representation of the setup is shown. A shaker is rigidly connected to a frame, which was designed for the application of the preload. The frame provides a static compression and the shaker provides a dynamic axial excitation.

The system under investigation consists of a circular cylindrical shell, made of aluminium, clamped both at the base and the top ends to rigid supports by means of rings (see Figure 1a.1). The geometric and physical parameters of the circular cylindrical shell are reported in tab. 1. The bottom support is an aluminum alloy thick circular disk rigidly bolted to the shaker. The top disk is connected to the frame by means of a dynamic load cell, a stinger, and a static load cell. The stinger is introduced in order to reduce the effects of misalignments. A laser vibrometer is used to measure the lateral vibration of the side of the shell and its output is routed both to the spectrum analyser and to the shaker controller. The control system is open-loop in order to avoid control instabilities induced by the nonlinear behavior of the system.

The press system presents a movement screw that can move up or down a plate (5 of Figure 1a) which applies the desired preload, both compressive and tractive. A static load cell “AEP transducers TC8 10KN” is connected with a digital load gauge that shows the actual preload applied to the shell. The Shaker “LDS V530” is rigidly integrated in the press system structure, see Figure 1b.

The specimen consists of a thin walled circular cylindrical aluminum shell. The specimen quality is crucial to have repeatable test: for this reason a specific procedure for preparing specimens has been followed. The production of the specimen starts from a standard beverage aluminum canister, which

Shell length	L	$0.117m$
Shell thickness	h	$0.15 \cdot 10^{-3}m$
Mean radius	R	$32.9 \cdot 10^{-3}m$
Density	ρ	$2796 \frac{kg}{m^3}$
Young's modulus	E	$71.02 \cdot 10^9 \frac{N}{m^2}$
Poisson's ratio	ν	0.31
Static preload	P_0	$0N - 250N$

Table 1: Geometry, load and mechanical properties of the shell

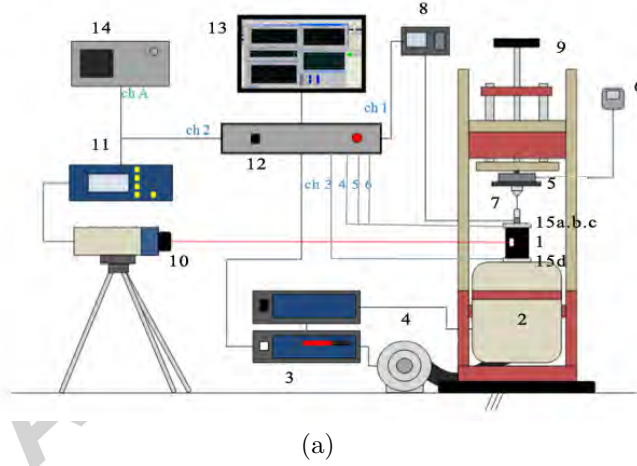


Figure 1: (a) system setup: (1) structure under test (2) shaker (3) shaker amplifier (4) air cool system (5) plate and static load cell (6) digital load gauge (7) force transducer PCB-M231B (8) force transducer amplifier (9) press system to apply static preload (10) laser vibrometer (11)laser controller (12) shaker control system (13) pc (14) spectrum analyzer ono-sokki CF-5220 (15a.b.c) 3 top accelerometers (15d) base accelerometer; (b) press system and shaker

must be suitably cut to obtain the desired dimension and eliminate the end diaphragms. The first step consists of refilling the empty canister with distilled water and put it in a climatic chamber at -10°C for two hours. After that, the frozen canister is cut at the required length without introducing any deformation. At the end, the specimen is rigidly connected to the two aluminum disks by means of two hose clamps interjected with a metallic band.

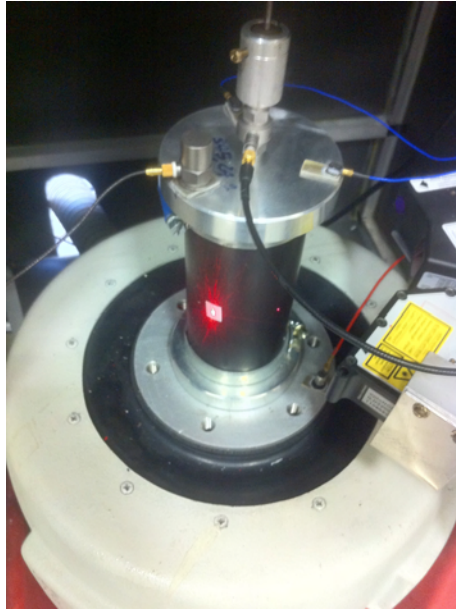
The system under investigation is equipped with several sensors, see Figure 2a:

1. A vibrometer is targeted on the shell surface and plays a significant role as it allows the measurement of the lateral shell vibration, in terms of normal velocity, without any mechanical contact and without altering the symmetry of the structure.
2. Three accelerometers are placed on the top disk, angularly spaced by 120° to measure the top acceleration, a fourth accelerometer is placed on the base. The accelerometers have been isolated with a fibreglass plate to prevent electric noise due to ground loop.
3. A dynamic load sensor has been placed between the top rigid disk of the shell and the press frame interject by a stinger to reduce the misalignment between the specimen and the frame.
4. A static load cell has been placed to control the compressive static load. It is worthwhile to point out that the static load cell and the force transducer are placed in series; therefore, assuming that the effects of the connection are negligible, the load cell measures the static part of the axial load and the force transducer measures only the oscillating part (it is piezoelectric and the acquisition is carried out in AC mode).

Moreover two Laser telemeters (displacement sensor) have been also installed to measure the lateral displacement of the shell.

3. Modal Analysis

A preliminary modal analysis has been carried out for better understanding the shell behaviour and for identifying the natural frequencies, damping ratios and modal shapes. A micro impact hammer was used for this purpose,



(a)



(b)

Figure 2: (a) press system and shaker; (b) impact hammer

see Figure 2b. The micro-hammer is a PCB Modally Tuned, ICP instrumented impact hammer. Micro accelerometers are used in conjunction with the hammer to perform a measurement of the structural response.

Modal analyses have been performed in the frequency band between 1100 and 2000 Hz, with three different levels of preload: 0 N, 50 N and 100 N. In the case of 0 N preload, a vertical series of 11 points is considered along the length of the specimen as well as a horizontal series of 20 points along the circumference, exactly at one half of the shell length. For 50 N and 100 N static compressive load analyses, two circumferential series of 20 points of measurement has been added at one-fourth and three-quarters of the shell length. All experimental data were post processed in order to obtain the synthesized FRF; the modal shapes were then reconstructed using a dedicated Matlab script.

In tab. 2 the measured natural frequencies are reported together with the description of the corresponding modal shapes. In this table m represents the number of axial half waves, while n is the number of nodal diameters.

It can be noted the presence of double modes, identified by the same pair of numbers (m, n) ; these modes should have theoretically the same frequency.

		Static axial load		
m	n	0N	50N	100N
1	6	1202	1198	1192
1	6	1205	1203	1196
1	7	1244	1238	1230
1	7		1249	1242
1	5	1391	1390	1384
1	5			
1	8	1456	1450	1443
1	8	1471	1456	1453
1	9	1754	1747	1741
1	9	1760	1755	1749
1	4	1866	1865	1861
1	4	1896	1893	1888

Table 2: Natural Frequencies [Hz] and mode shape description.

In the real case, due to the presence of imperfections, double modes generally split into two modes having the same shape (shifted of a quarter of period circumferentially) and similar frequency. For some modes it was impossible to find experimentally the two conjugate (double) modes, this happens typically when the frequency splitting is not enough to distinguish the conjugate modes.

The effect of 100N preload on the natural frequencies is about 1%, this is expected as the buckling load of the present shell is about 6100N, therefore the theoretical prediction of the frequency variation is coherent with the experimental findings, see Ref. [28]. Nonetheless, such small linear effect of the preload produces significant effects on the dynamic response when the system vibrates in nonlinear regime.

3.1. 0N preload

Figure 3 shows the reconstructed modal shapes in 3D and map visualization for the fundamental mode (1,6), the measured points have been plotted as blue circles and the other data, due to the shell symmetry, were interpolated. Figure 4 shows the other mode shapes, for the sake of brevity only the map visualization is represented.

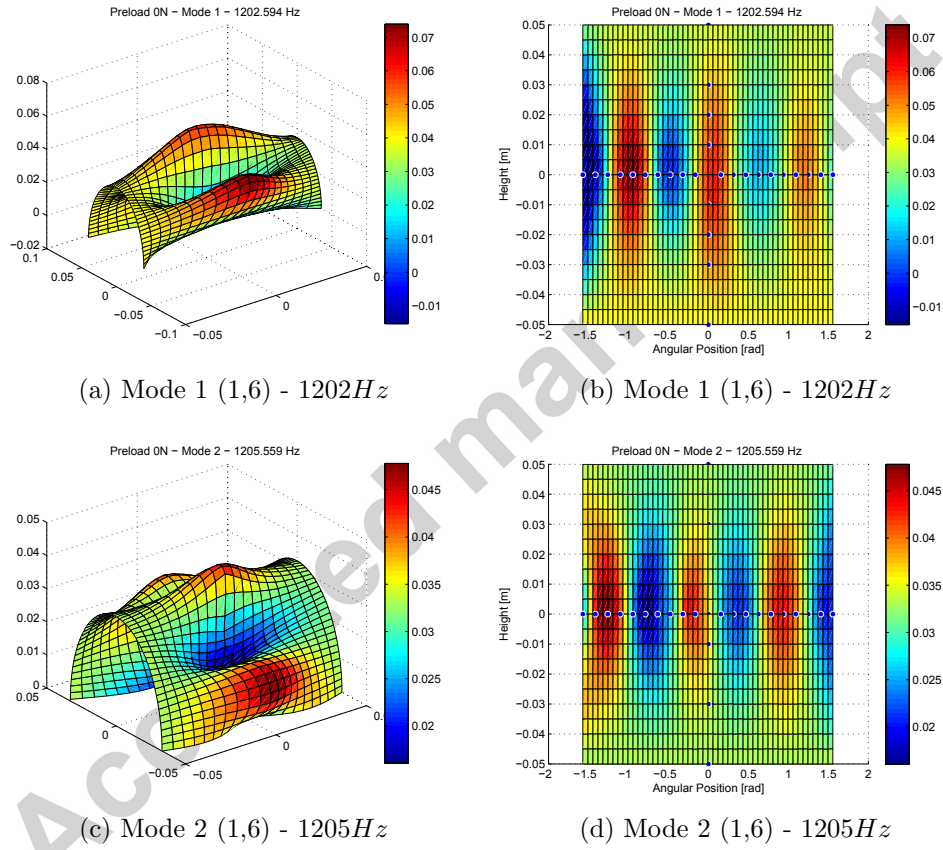


Figure 3: Modal Shape - 0N preload

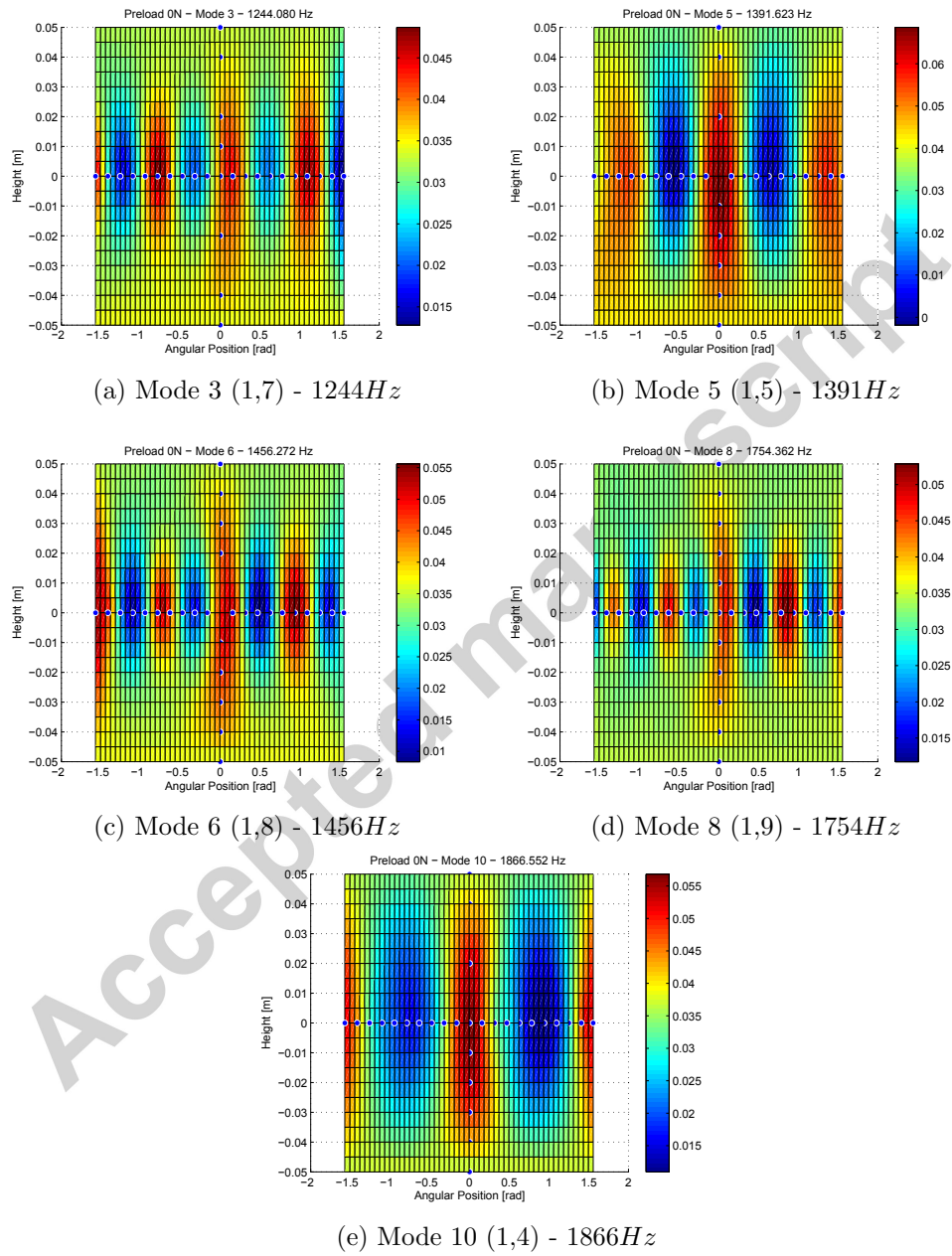


Figure 4: Modal Shape - 0N preload

4. Nonlinear dynamics: experimental results and discussion

In this section, experiments performed with a combined static and dynamic load will be shown. Since the occurrence of nonlinear effects due to the high lateral displacement of the shell is expected, it is important to choose a suitable test strategy. The dynamic load is harmonic and the frequency is varied following a sine step procedure; the peculiar feature of the sine step is that a smooth sine step test is applied; indeed, standard sine step controllers (e.g. LMS TestLab) do not guarantee C^1 continuity in the waveform when the frequency is changed, this is acceptable for standard testing, but it is not enough in nonlinear field where multiple states are possible and the basins of attraction can be small; in these cases also a small perturbation can lead to a jump from a stable state to another one; therefore, we propose a sine step excitation with C^2 frequency variation. Therefore, the following procedure is used:

- test is started at the initial frequency f_0 and a certain number of excitation periods at f_0 are generated;
- only the last periods at f_0 are stored for performing analyses, i.e. the transient is eliminated;
- frequency is varied from f_0 to $f_1 = f_0 + \Delta f$ using a sine sweep;
- the signal is smoothly connected with a new signal at f_1 frequency and a certain number of periods are generated at the frequency f_1 ;
- only the last periods at f_1 are stored for performing analyses;
- frequency is varied again at $f_2 = f_1 + 2\Delta f$ using a sine sweep, and this procedure is iterated up to the last frequency.

The output is generated by means of the "Waveform replicator" of TestLab, a full waveform of the output (including the smooth frequency change) is generated by Matlab and imported in TestLab, which generates the desired output (in voltage). In the experiments, the sine step excitation range goes from 1100Hz to 2000Hz, with a frequency step of 1.0 Hz. For some special region, a finer step of 0.1Hz is used. Each run starts at the highest frequency (2000Hz) towards the lower frequency (1100Hz) and then it goes back to the highest frequency. Several excitation levels are considered in terms of voltage

amplitude applied to the shaker amplifier. Amplitude range is between 0.1 and 1V, with 0.1 V increment.

Different axial pre-loads are considered: $P_0 = 0N$, $P_0 = 100N$ and $P_0 = 250N$ (max shaker load capacity).

During the tests the following physical quantities are measured:

- the base acceleration, by means of an accelerometers placed on the shaking table;
- the dynamic axial load, by means of a piezo-electric load cell;
- the lateral vibration, by means of a laser vibrometer;
- the acceleration of the top mass, by means of three accelerometers placed at 120° angle.

5. 0N preload

In Figure 5 the three accelerations on the top disk (called top1, top2 and top3) are compared with the base acceleration for two excitation levels 0.1 and 1V. Downward and upward frequency variations are identified by labels "down" and "up" respectively.

It can be noticed a proportionality between the magnitude of the forcing load and the response; an amplification factor of the response of three times at the resonance is observed.

The top1 and top3 accelerations present different behaviors with respect to the top2 acceleration (the latter is one-third lower), such difference indicates a top disk tilt. A perfect system should not undergo to top disk tilt due to the symmetry, in real conditions the tilt can take place due to unavoidable small misalignments of the top rigid disk with respect to the stinger, such misalignments activate beam-like modes of the shell. In fact, the imperfect alignment of the stinger, with respect to the fixture of the rigid disk, causes an imbalance of the axial load with a consequent tilt of the top disk.

In Figure 6 the dynamic load of the shell is shown for excitation levels 0.7V and 1.0V (downwards and upwards); for both tests one can observe that the amplitude is proportional to the excitation level, this confirms the linear behavior in such conditions. For the same test conditions, the lateral velocity is presented in Figure 7, it can be noticed a slight softening behavior; for the 0.1V case, Figure 7a. The presence of double modes is clearly visible

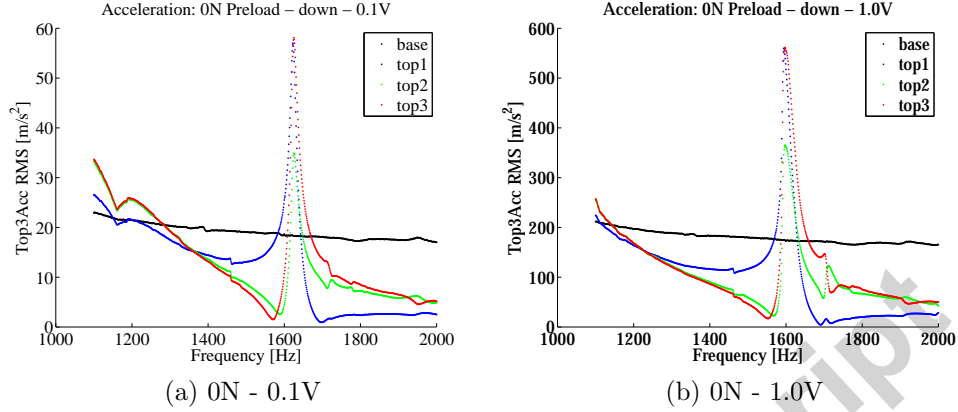


Figure 5: Amplitude-frequency diagrams of accelerations - 0N

around 1200Hz, where a double peak is present; at higher excitation levels the double modes are no more visible, this is probably due to the dominant nonlinear effects that couple the companion modes into a combined response close to their resonance.

6. 100N preload

If the preload is increased up to 100N, interesting phenomena arise. For this reason, in order to provide a clear description of the dynamic scenario, the amplitude-frequency diagrams (Figure 8) are accompanied with the bifurcation diagrams of the Poincaré maps and the waterfall diagrams of the spectra, Figure 9.

Figure 8a shows the acceleration at the top (three accelerometers) and the base, for the excitation level 0.1V; the main linear resonances are clear peaks having a slight asymmetry close to 1200Hz, due to nonlinear effects. Again the three top accelerometers show different amplitudes, proving the presence of a tilt. When the excitation level is higher (1V, Figure 8b) nonlinear effects are pronounced only for the resonance close to 1200Hz; this behavior is clarified by the analysis of the dynamic axial load measurement (Figure 8d), which shows a huge load magnification around 1200Hz.

The strong nonlinear character of the response is clearly visible in Figures 8c and 8d, where a saturation phenomenon is present at the highest levels of preload (about 60N) around the resonance at 1200Hz. The nonlinear response is confirmed by the lateral vibration represented in Figures 8e and

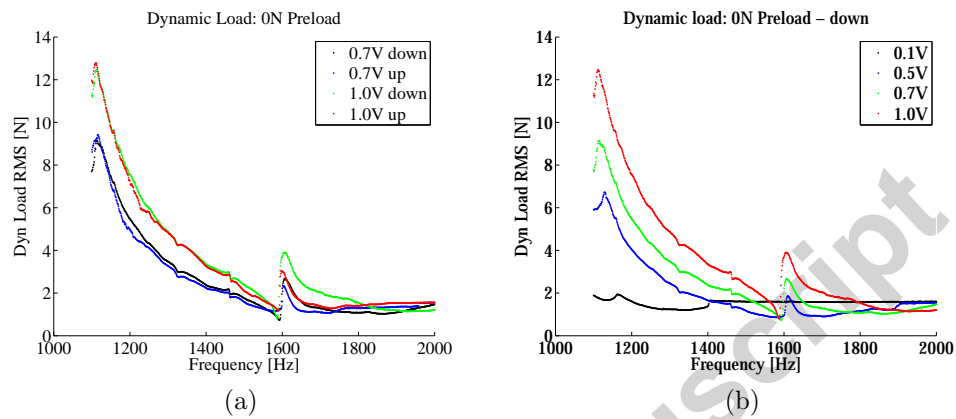


Figure 6: Amplitude-frequency diagrams of the dynamic load - 0N

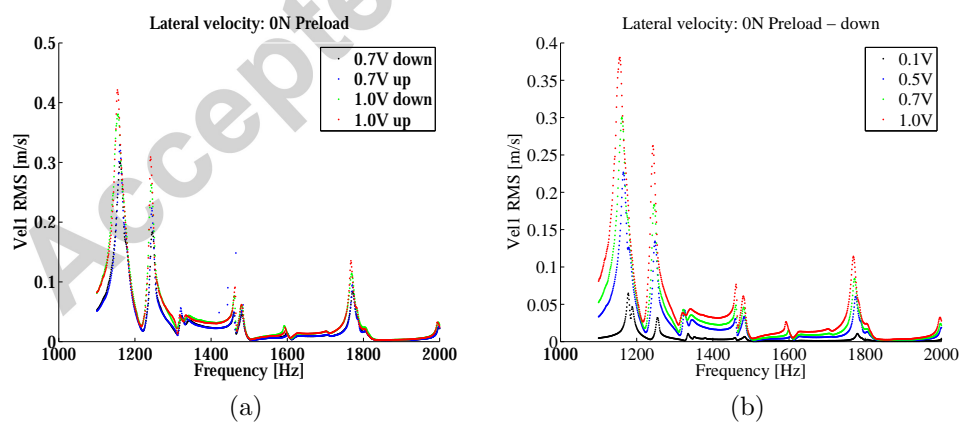


Figure 7: Amplitude-frequency diagrams of the lateral velocity - 0N

8f; here it is clarified that the excitation of the lateral vibration gives rise to the nonlinearity, jump phenomena are observed for 0.5-1.0V drive levels both for the downward and upward tests. In Figure 8d the dynamic load response looks like squeezed as if a threshold was present, this is due to nonlinear effects and energy transfer to the lateral vibration (shell like). In fact, one can observe a large and non-proportional increment of the lateral velocity with the forcing load intensity, see Figure 8e; close to 1150Hz there is a gap between the case at 0.1V and the cases at 0.5-1.0V, at higher excitations there is no difference in terms of amplitude. Close to 1200Hz the situation is different, there is a regular increment of vibration with the excitation level; only the 1V excitation shows a jump vs. frequency; this is due to the nonlinear response (here softening) that gives rise to a saddle node bifurcation. Figure 8f proves that the most interesting dynamics take place below 1300Hz. The nonlinear effect in the response is present from 0.5V drive with a jump and a softening behavior, see Figure 8e; at 1.0V a frequency gap in the jumps (about 10Hz) is present between downwards (red line) and upwards (light green line) runs.

In Figure 9 bifurcation diagrams of the Poincaré maps and waterfall diagrams of the power spectrum of the lateral vibration are represented. The waterfall diagrams are presented in logarithmic colormap (red-yellow are the highest and blu-light green the lowest); the forcing frequency step is 1Hz on the vertical axis.

The bifurcation diagrams of Poincaré maps give a qualitative important information about the dynamic scenario. If one follows the diagram, by varying the horizontal parameter, different situations can be found: a single line/curve means periodic response (also in presence of superharmonics), for each frequency this means that the Poincaré map is one single point; two co-existing curves mean subharmonic response of period two ($2T$); m coexisting curves mean mT subharmonic response; a non quantifiable number of points at a specific frequency means non-periodic response (*e.g.* quasiperiodic or chaotic).

If waterfall diagrams are referred to systems with some cyclicity, *e.g.* periodic forcing, the excitation frequencies are represented by straight inclined lines (the angular coefficient of the fundamental frequency is one, for superharmonics consider multiples). If lines are present symmetrically with respect to a forcing it means the presence of sidebands (quasiperiodic response); vertical lines represent resonances; horizontal lines represent broadband spectra (random like).

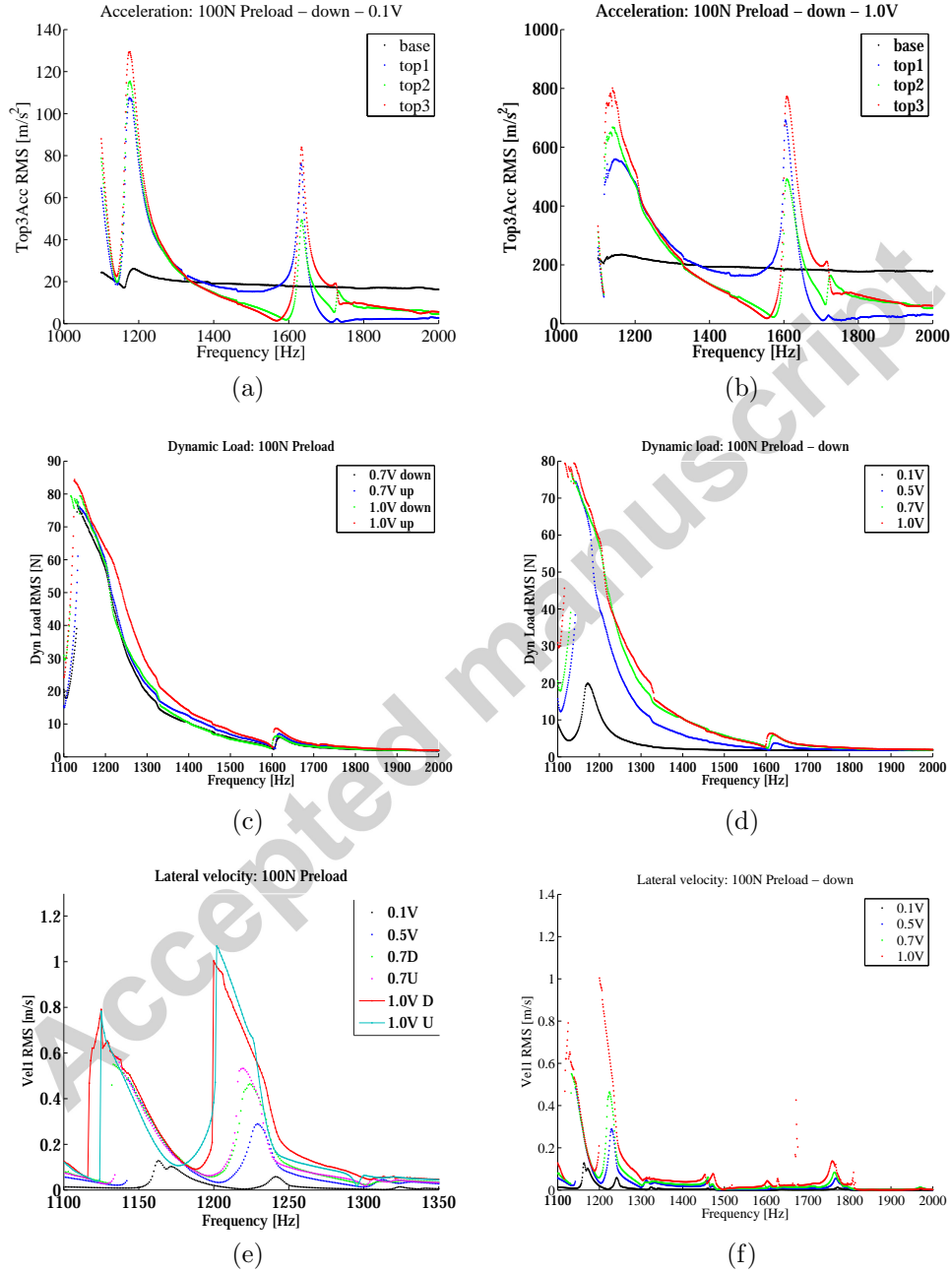
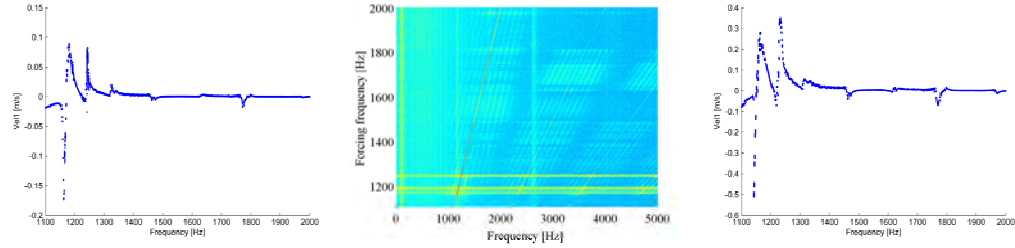


Figure 8: Amplitude-frequency diagrams at 100N preload: (a,b) acceleration; (c,d) dynamic load; (e,f) lateral velocity

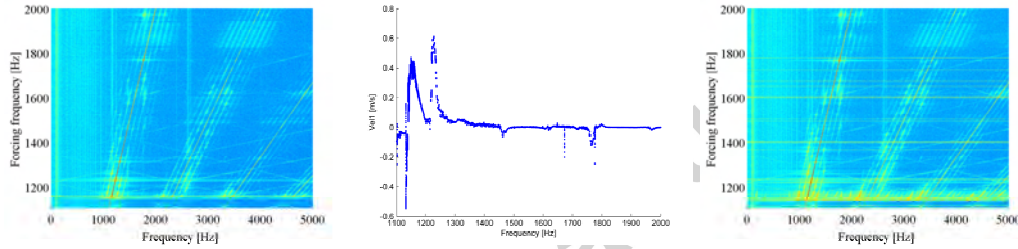
For the cases 0.1-0.5V drive the bifurcation diagrams of the Poincaré maps, Figure 9, show single curves, *i.e.* periodic response. For 0.7-1V drive the situation is similar except for a narrow region close to 1150Hz, where the diagram shows a dispersed cloud of points, here a quasiperiodic or chaotic motion is present; taking advantage from the corresponding waterfall diagram, it is clear that the motion is quasiperiodic as sidebands are visible.

For the case of 1V drive, downwards, the complex dynamics is characterized by a broadband spectrum which can be found also at high frequency of excitation.

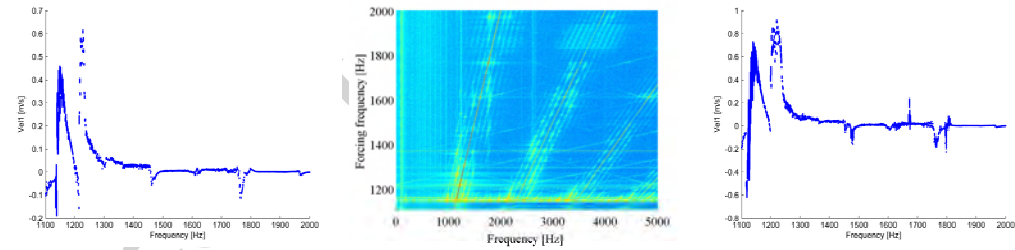
In the following, a detailed description of the dynamic scenario is given in terms of 2D Poincaré maps, 2D phase portraits, spectra and time histories. These analyses are focused to the most interesting regimes, full data are available in ref. [29].



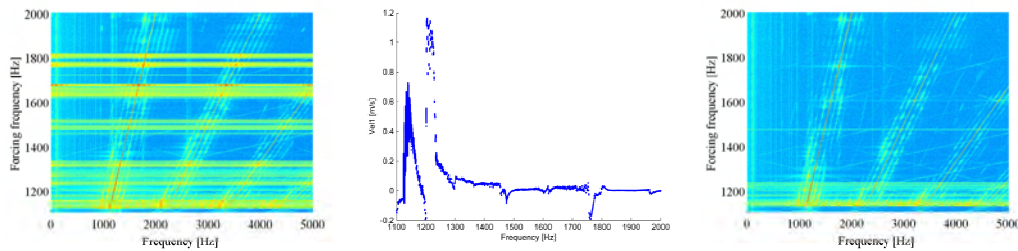
(a) Bifurcation diagram of the Poincaré maps at 0.1V downwards
(b) Waterfall diagram at 0.1V downwards
(c) Bifurcation diagram of the Poincaré maps at 0.5V downwards



(d) Waterfall diagram at 0.5V downwards
(e) Bifurcation diagram of the Poincaré maps at 0.7V downwards
(f) Waterfall diagram at 0.7V downwards



(g) Bifurcation diagram of the Poincaré maps at 0.7V upwards
(h) Waterfall diagram at 0.7V upwards
(i) Bifurcation diagram of the Poincaré maps at 1.0V downwards



(j) Waterfall diagram at 1.0V downwards
(k) Bifurcation diagram of the Poincaré maps at 1.0V upwards
(l) Waterfall diagram at 1.0V upwards

Figure 9: Bifurcation diagram of the Poincaré maps and waterfall diagram of power spectrum - Lateral velocity - 100N preload (continued from previous page)

6.1. 0.7V Downwards

In the present section, downward tests in a frequency band close to 1140Hz are described in detail. The shell is pre-loaded at 100N and the amplitude of the dynamic excitation (drive) is 0.7V . Poincaré sections and phase portraits are represented by means of (base acceleration, lateral vibration) and (dynamics axial load, lateral vibration) planes; this is not the typical representation, i.e. (displacement, velocity) of the same point); indeed, no direct measurement was available and we preferred not to use transformed data of the same time history (for example numerical derivation or integration). In our opinion such kind of representation is as effective as the traditional one, because the physical quantities used are related to the same dynamic phenomenon. In Figure 10 Poincaré maps and phase portraits are represented in the plane (base acceleration, lateral vibration), spectra and time histories are related to the lateral velocity of the shell. In Figure 11 Poincaré maps and phase portraits are shown in the plane (dynamic axial load, lateral vibration), spectra and time histories are related to the dynamic axial load.

From 1134 to 1142 Hz quasiperiodic responses are evident (cases *i* – *iii* of Figure 10). A small frequency variation (1Hz) from 1143 to 1142Hz determines a sudden change of the dynamic character, the map becomes fractal; since the test is performed downwards, this means a collapse of a chaotic attractor into a quasiperiodic one.

At 1139Hz the dynamic load shows strong sub-harmonics in the spectrum, but the response is quasiperiodic, this is confirmed also from the phase portrait and the Poincaré map.

From 1144 to 1143Hz a sudden transition to chaos takes place, at 1143Hz the map appears irregular, the phase trajectory fills a portion of the phase space. Increasing or decreasing the frequency of just 1Hz from 1143Hz, the chaotic character suddenly disappears, see the case at 1144Hz; it is interesting to see that no apparent change of response quality is visible in the lateral vibration time histories and spectra.

6.2. 1.0V Downwards

In Figure 12 and in Figure 13 downward tests at 1V drive and 100N preload are analyzed.

At 1117Hz a small modulation is present, it is visible both in the time history and the spectrum, but Poincaré map and phase trajectory do not show any peculiar behavior. From 1121Hz the modulation is more pronounced,

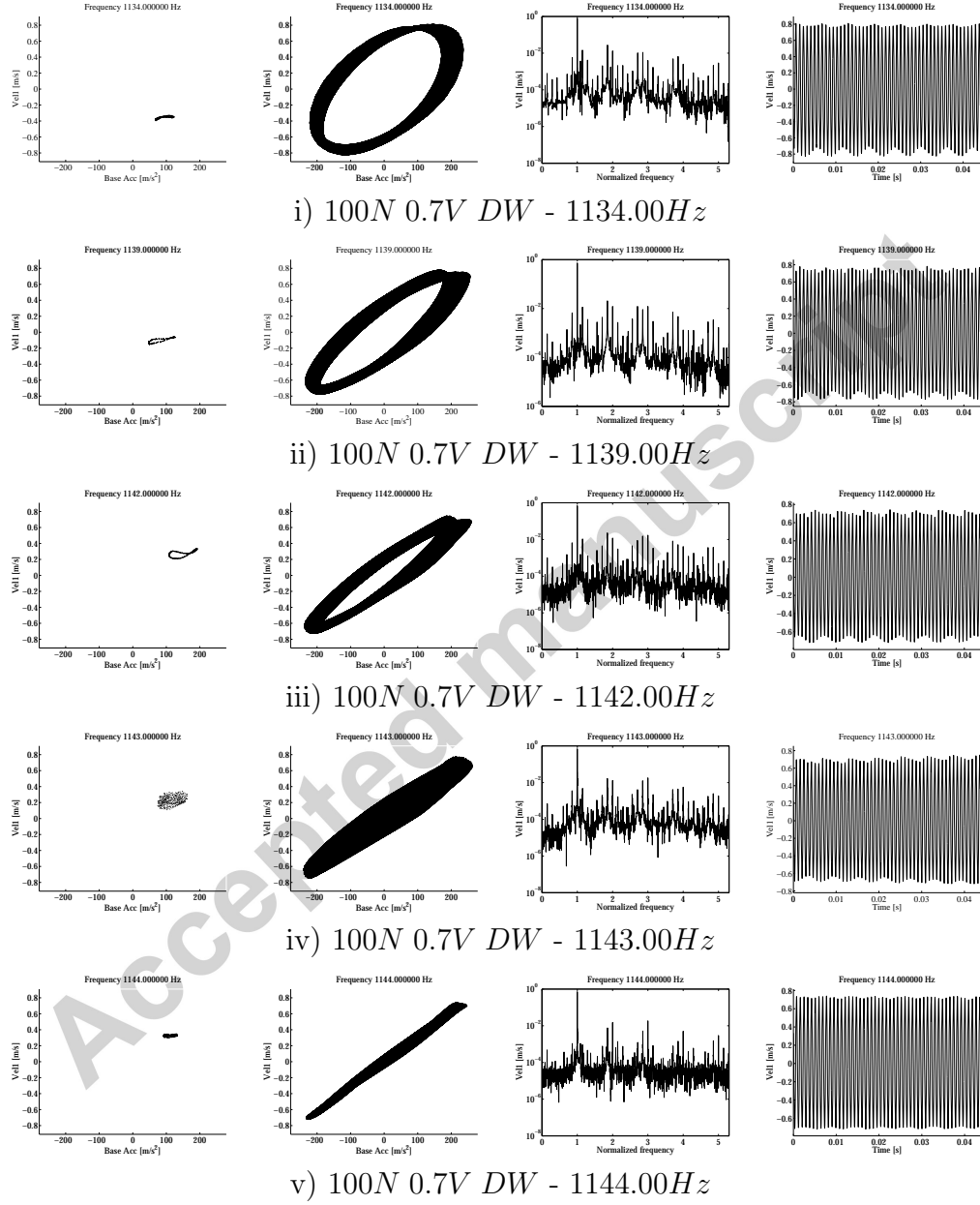


Figure 10: Base acceleration - Lateral velocity: Poincaré maps, phase portraits, spectra and time histories at 100N 0.7V downwards

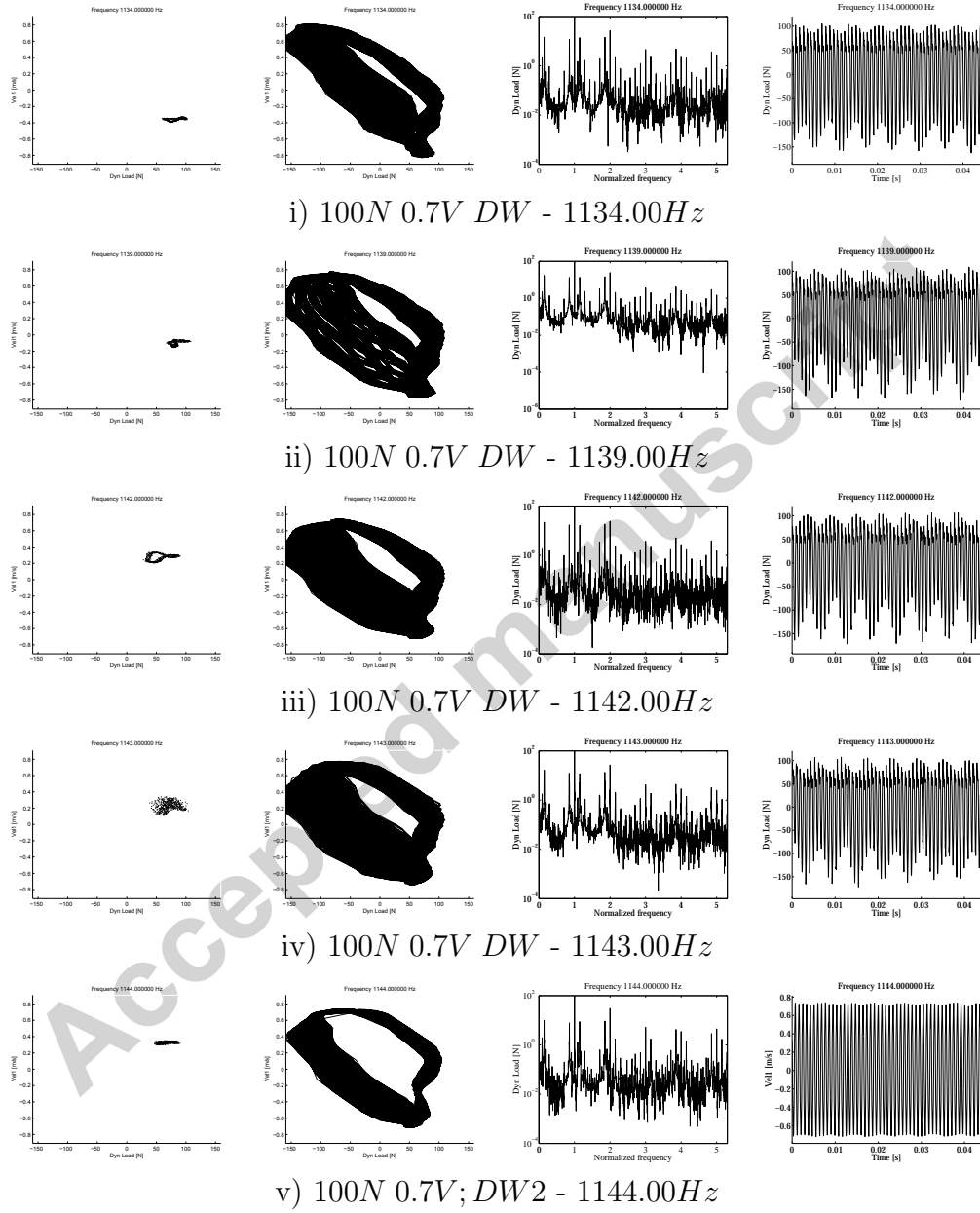


Figure 11: Dynamic load - Lateral velocity: Poincaré maps, phase portraits, spectra and time histories at 100N 0.7V downwards

this is now confirmed by a Poincaré map developed on a one dimensional set, the shape is the typical ∞ type due to some twist. From 1125 to 1130Hz the initial shape of the Poincaré map is deformed, it seems that twin 1D attractors coexist and the dynamical system continually jumps from one to the other attractor. The quasi-periodic attractor (lateral vibration) seems to coexist with a chaotic attractor (dynamic force), i.e. the response of dynamic load shows a chaotic response, the Poincaré map up presents a fractal aspect. At 1134Hz a strongly subharmonic response of period 20T suddenly appears, the Poincaré map seems unchanged, but it is not continuous anymore, now it is made of 20 points. The conclusion is that between 1133Hz and 1135Hz there is a transition between quasi periodic motion, 20T subharmonic response, and quasi periodic motion again. It is to stress that the shape of the 20T subharmonic attractor at 1134Hz is made of 20 points located exactly on the shape of the continuous map found at 1133 and 1135Hz; it seems that the quasiperiodic 1D attractor collapses (for a while) on a subharmonic 0D (zero dimensional) attractor. The same transition can be observed on the Poincaré maps in the plane (dynamic axial load, lateral vibration), Figure 13: in this case the presence of a subharmonic motion is clearly visible at 1134Hz, even though counting the periodicity is less easy due to the larger uncertainty in the measured dynamic load. At 1133 and 1135Hz the response is quasiperiodic.

The collapse of the quasiperiodic attractor into a strongly subharmonic attractor is quite interesting and can be fully justified by the analysis of the waterfall diagram of Figure 9j, here several sidebands can be found, most of them follow the fundamental excitation frequency maintaining the distance unchanged; however, close to 1150Hz one can see that the distance of some sidebands varies, they tend to move toward the fundamental frequency; therefore, it is obvious during such a distance variation, some sidebands will meet some rational relationship with the fundamental excitation frequency. For 1134Hz drive frequency what happens is the following: the Poincaré map indicates a period 20T subharmonic response, this means that the fundamental frequency of the response is $1134/20 = 56.7Hz$, the analysis of the spectrum confirms the presence of a small (almost negligible) peak at $56.7Hz$, the response present the first left sideband exactly at $17/20 \times 1134Hz$, all other peaks are multiples of the $56.7Hz$. The time signal is quite peculiar, it is a periodic signal characterized by a very marginal contribution of the fundamental harmonics and its first multiples, even though the first harmonics of such a signal approach zero, it preserve its periodicity as all other harmonics

are multiples of the fundamental one.

A similar transition is present at 1148Hz: the system presents a subharmonic response both at 1147 and 1149Hz, while the response at 1148Hz is quasiperiodic.

This scenario reveals a very intricate bifurcation mechanism with the coexistence of different attractors.

Accepted manuscript

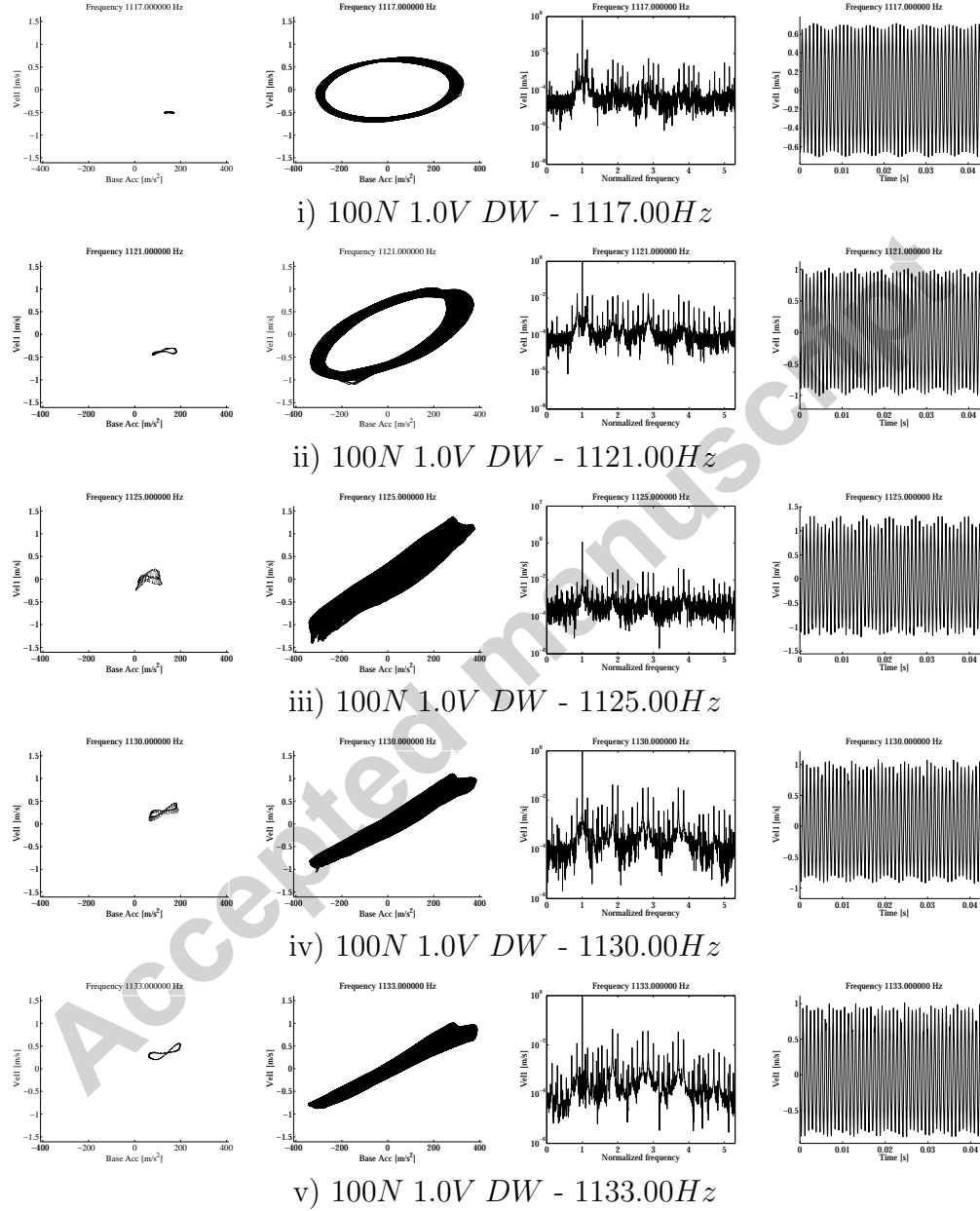


Figure 12: Base acceleration - Lateral velocity: Poincaré maps, phase portraits, spectra and time histories at 100N 1.0V downwards (continued on next page)

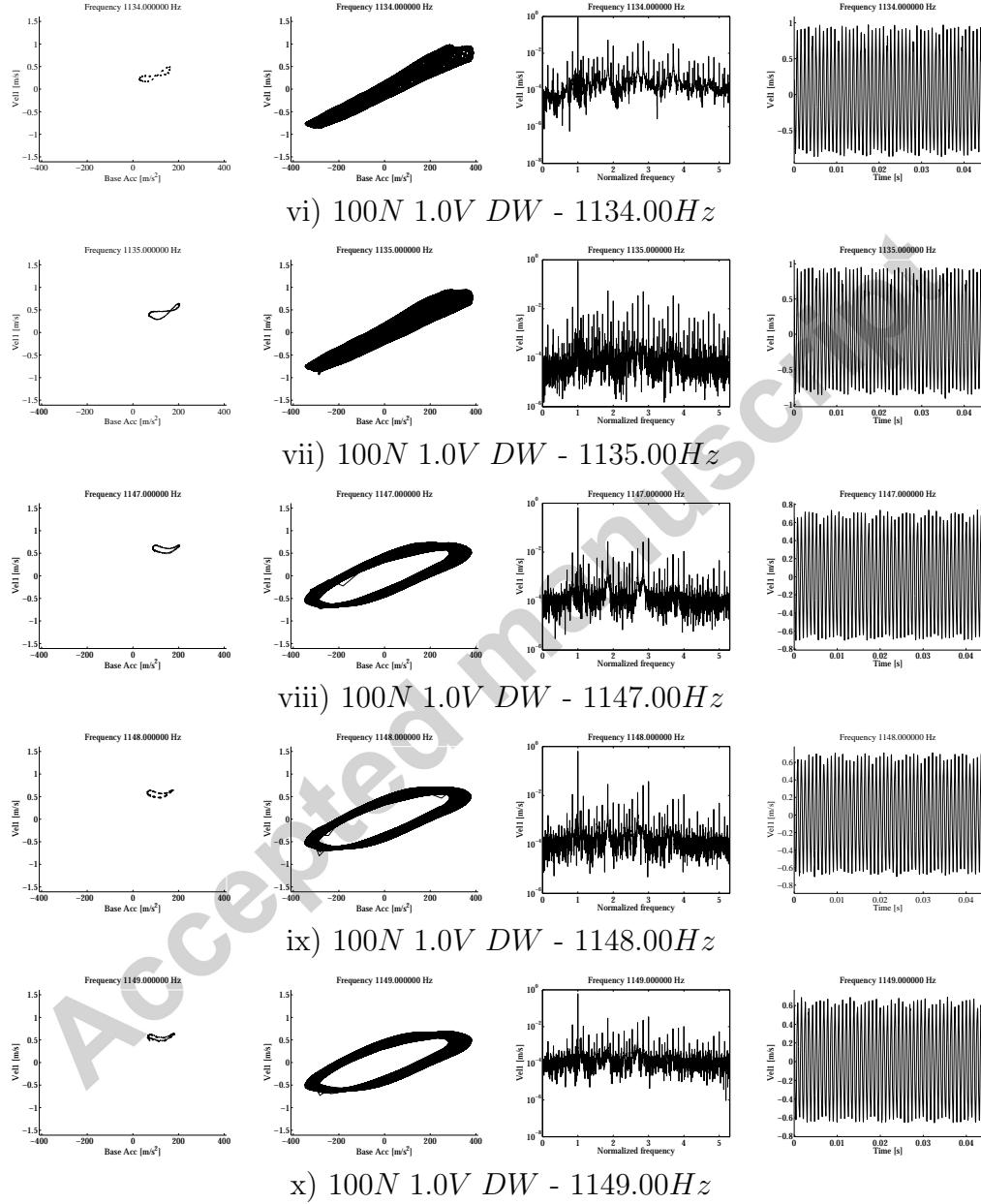


Figure 12: Base acceleration - Lateral velocity: Poincaré maps, phase portraits, spectra and time histories at $100N$ $1.0V$ downwards (continued from previous page)

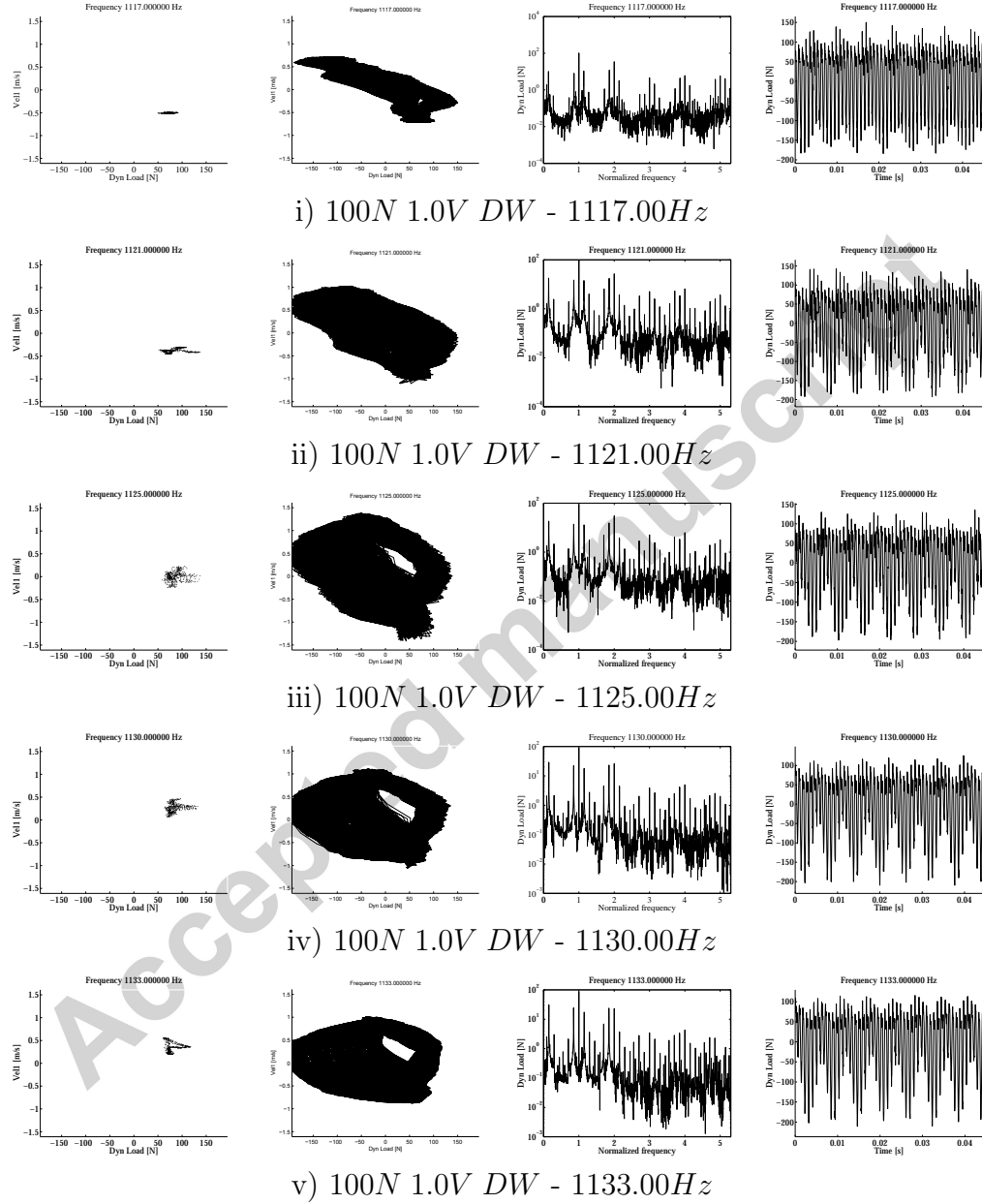


Figure 13: Dynamic load - Lateral velocity: Poincaré maps, phase portraits, spectra and time histories at 100N 1.0V downwards (continued on next page)

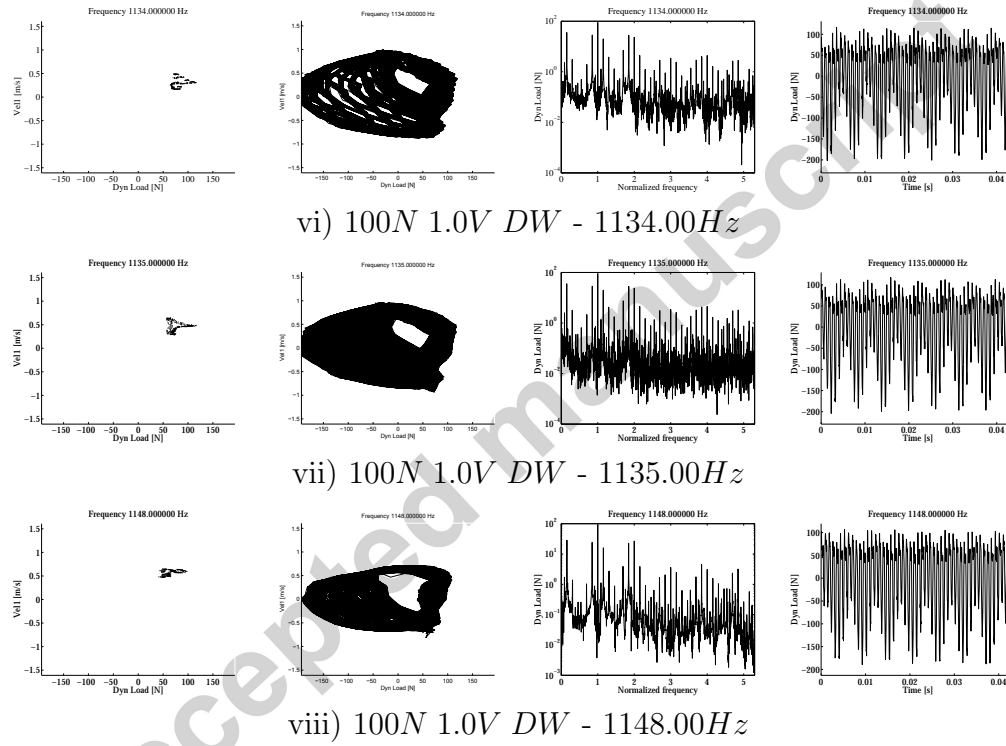


Figure 13: Dynamic load - Lateral velocity: Poincaré maps, phase portraits, spectra and time histories at 100N 1.0V downwards (continued from previous page)

6.3. 1.0V Upwards

In the present section, upward tests are analyzed. The static preload is $100N$ and the forcing amplitude is $1.0V$ (drive), see Figure 14. At $1124Hz$, a regular harmonic response both for velocity and dynamic load is observed. These results are presented to have a reference point and to quantify the underlying noise. Increasing the drive frequency of $1Hz$, from $1124Hz$ to $1125Hz$, the response becomes quasi periodic, there is a violent transition just after the jump, the lateral velocity jumps from a peak to peak amplitude of $0.12m/s$ to $2m/s$, see time histories of cases 1124 and $1125Hz$ and the corresponding amplitude-frequency diagram, Figure 8e. At $1126Hz$ a quasi-periodic response is completely developed, this behavior is unchanged up to $1154Hz$, where the shell vibration appears periodic and strongly sub-harmonic. At $1155Hz$ the response is quasiperiodic again.

The representation of the dynamics in terms of dynamic load for the same cases present clear chaoticity, except at $1124Hz$, i.e. before the jump to the instability. A well defined chaotic response is evidenced from the Poincaré map projected on the plane (dynamic axial load, lateral vibration), conversely, the projection on the plane (base acceleration, lateral vibration) shows a quasi periodic response. The lateral vibration seems to be quasi periodic and the response of the dynamic load chaotic: this could be explained with a different response between the lateral response and axial response, and if we look back to the amplitude frequency diagram we can note two resonances for the lateral velocity and only one for the dynamic load, see Figures 8e and 8c. It seems that the system responds with two coexisting types of dynamics; this is a strong conjecture that would need a theoretical interpretation.

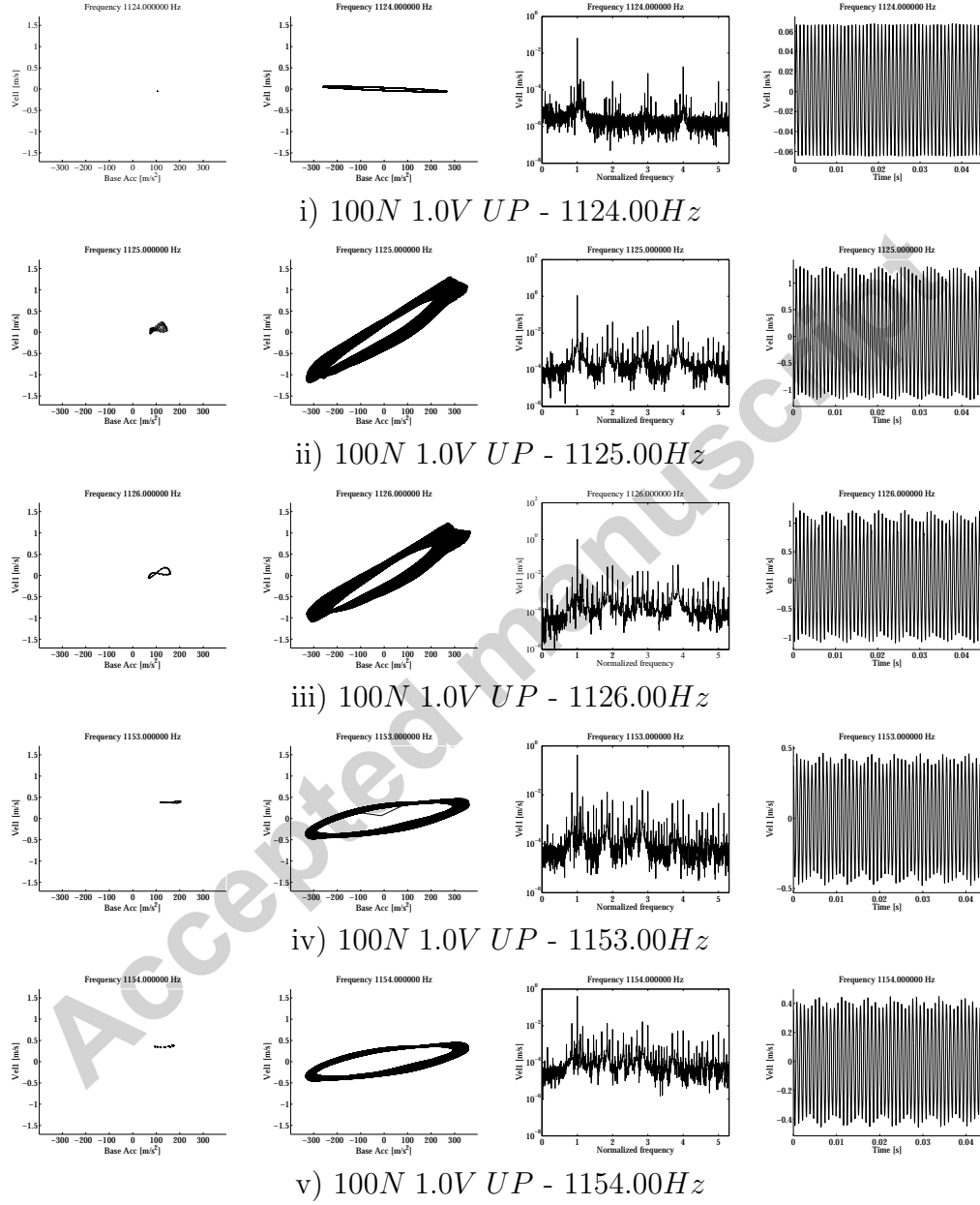
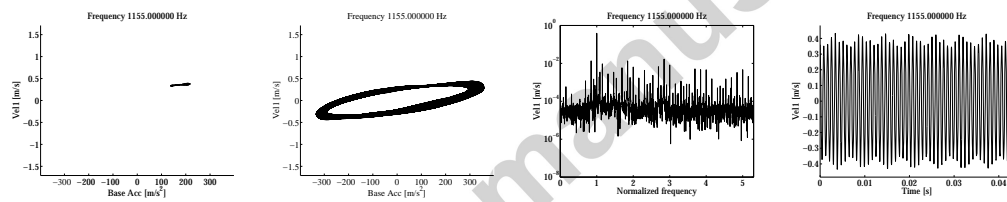


Figure 14: Base acceleration - Lateral velocity: Poincaré maps, phase portraits, spectra and time histories at 100N 1.0V upwards (continued on next page)



vi) $100N$ $1.0V$ UP - $1155.00Hz$

Figure 14: Base acceleration - Lateral velocity: Poincaré maps, phase portraits, spectra and time histories at $100N$ $1.0V$ upwards (continued from previous page)

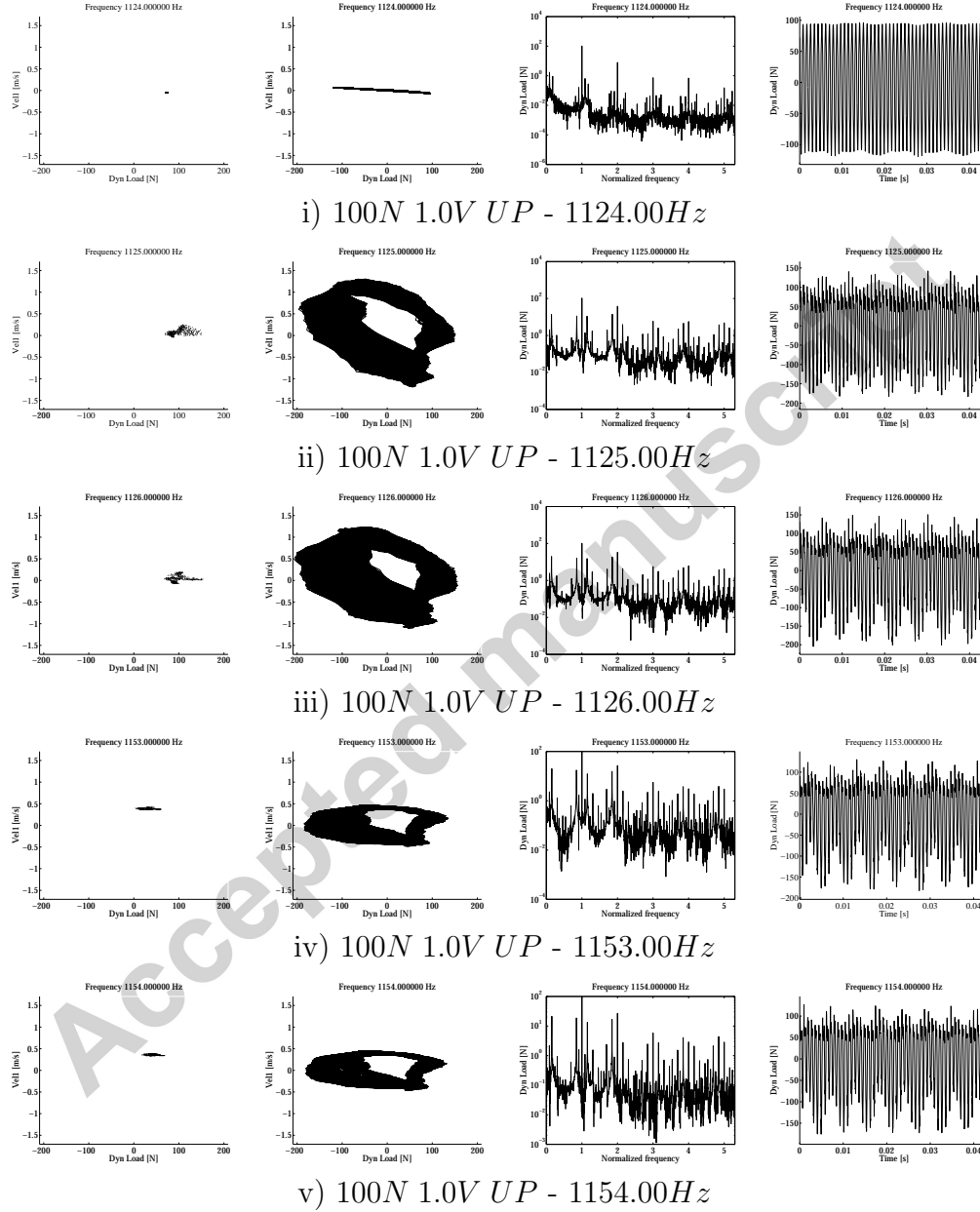
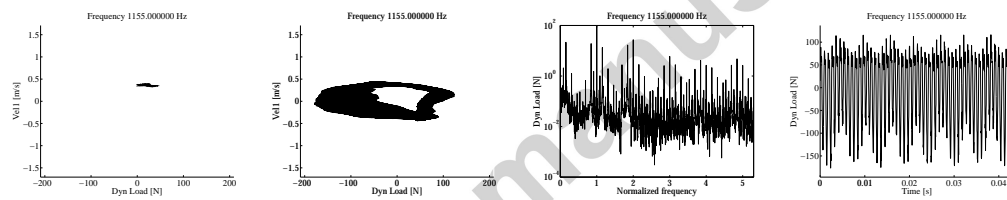


Figure 15: Dynamic load - Lateral velocity: Poincaré maps, phase portraits, spectra and time histories at 100N 1.0V upwards (continued on next page)



vi) $100N$ $1.0V$ DW - $1155.00Hz$

Figure 15: Dynamic load - Lateral velocity: Poincaré maps, phase portraits, spectra and time histories at $100N$ $1.0V$ upwards (continued from previous page)

7. 250N preload

At the maximum preload, several violent phenomena occur: for better describing the most interesting nonlinear behaviors of the shell under this condition, additional tests have been performed. In particular, downwards and upwards tests have been repeated increasing the frequency resolution from 1 to 0.1Hz and time of acquisition up to 1500 periods for each frequency (in the range 1160-1290Hz), these refined tests are identified as run 2 (both upwards and downwards).

Comparing the amplitude-frequency diagrams at 100N and 250N (Figures 8 and 16), one can observe an increment of the maximum top acceleration of 150% at 0.1V drive and 160% at 1.0V drive; the increment in terms of maximum dynamic axial load is 300%; while the maximum lateral vibration has only a marginal increment.

The top acceleration, shows regular resonances at 0.1V drive (Figure 16a), whereas for the drive voltage of 1V (Figure 16b) close to 1200Hz a saturation appears and the amplitude remains almost constant up to 1170Hz, then suddenly the top vibration drops down to the level of the base vibration. This is a clear symptom of a strong nonlinear modal interaction.

Looking at the dynamic axial load (Figure 16c), the previous conjectures are confirmed; both up and down tests give similar results and no jumps are observed. Close to 1200Hz one finds the main resonance, it is to note that the maximum amplitude of axial load is not proportional to the drive, this is unexpected; comparing also Figure 16d) one can see that, far from the resonance at 1200Hz, the axial load amplitude is proportional to the drive, but close to such resonance up to 0.7V drive one sees a regular growth, then a huge increment is observed when the drive is increased up to 0.9V.

The second test (run 2) is carried out with a reduced drive frequency step (0.1Hz), this allows to follow complex phenomena with more detail (see Figure 16e run2); indeed, in a narrow frequency band close to 1200Hz a saturation phenomenon is visible on the dynamic load. The two tests at 1Hz and 0.1Hz give different scenarios of the dynamics as two stable attractors coexist.

The analysis of the lateral vibration clarifies what happens, see Figures 16f and 16g. For a drive voltage between 0.1 and 0.7V one can see several resonances, very regular and linear, the principal (largest amplitude) is at 1200Hz; for 0.9 and 1.0V drive there is a sudden enlargement of the frequency band where big amplitude of vibration is detected; moreover, tests carried out

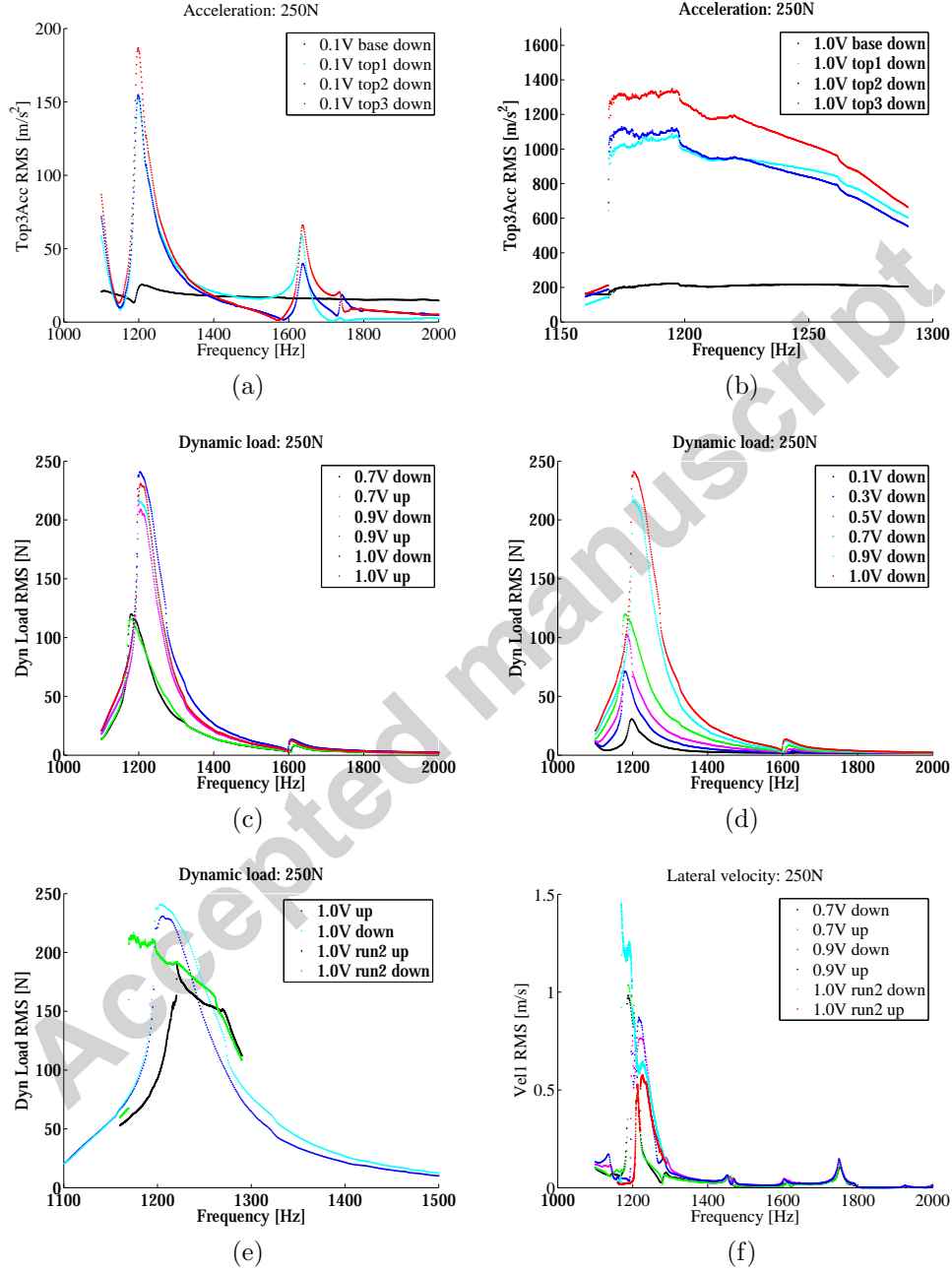


Figure 16: Amplitude-frequency diagrams at 250N preload: (a,b) acceleration; (c-e) dynamic load; (f-h) lateral velocity (continued on next page)

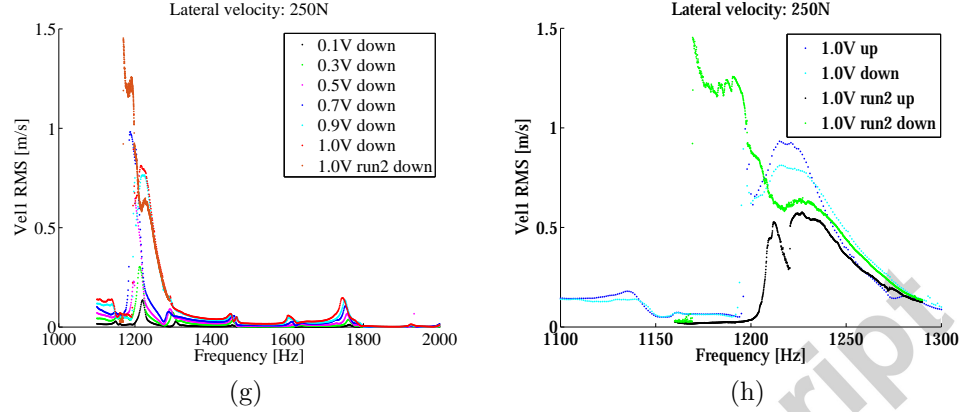


Figure 16: Amplitude-frequency diagrams at 250N preload: (a,b) acceleration; (c-e) dynamic load; (f-h) lateral velocity (continued from previous page)

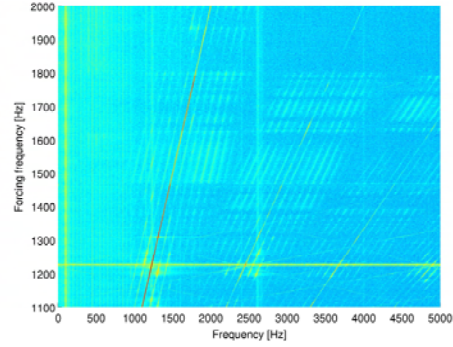
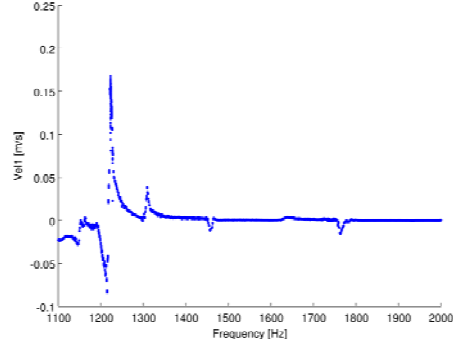
with 0.1Hz drive step give a further 50% increment of the maximum vibration level with respect to the case with 1Hz step. This proves that a strong nonlinear phenomenon appears and it is quite sensitive to the perturbation of initial conditions .

The scenario is clarified in the zoom of Figure 16h; tests carried out with 1V drive amplitude and 1Hz step give up to 1m/s lateral vibration, while tests with 0.1Hz step return 1.5m/s; moreover, the refined analysis with 0.1Hz shows an enlargement of the frequency band where big vibrations are detected. Eventually, using 0.1Hz step one observes a clear difference between upward and downward tests, with a large region (1130-1200Hz) where the system can respond with two different behaviors and amplitudes, jumps are present of course, the behavior is softening.

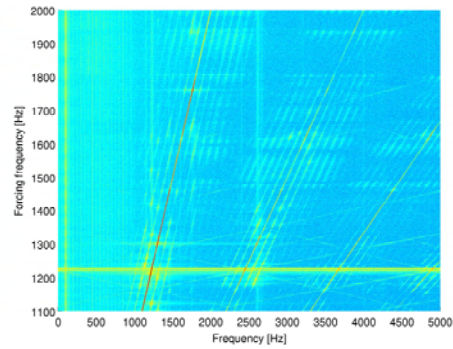
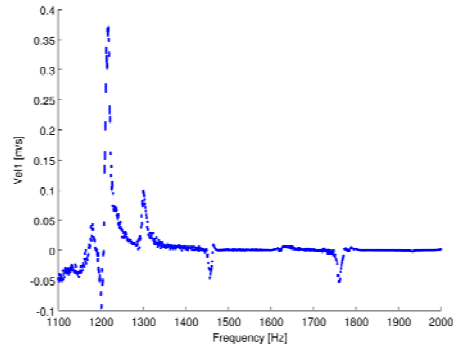
For the case of 250N preload, the bifurcation diagrams of the Poincaré maps and the waterfall spectrum diagrams are shown in Figure 17. The analysis of these diagrams shows that the response is periodic until 0.9V. For 0.9V drive amplitude, the bifurcation diagram presents a single vertical line close to 1200Hz; at the same frequency the waterfall diagram shows a broad band response with a clear presence of sidebands, this suggests the presence of a quasiperiodic motion.

The additional test (run 2), performed at an amplitude of 1V drive amplitude and with a refined frequency step of 0.1Hz, is extremely interesting; the response is different with respect to the run performed with 1Hz fre-

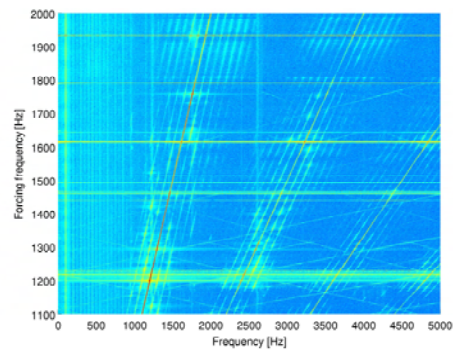
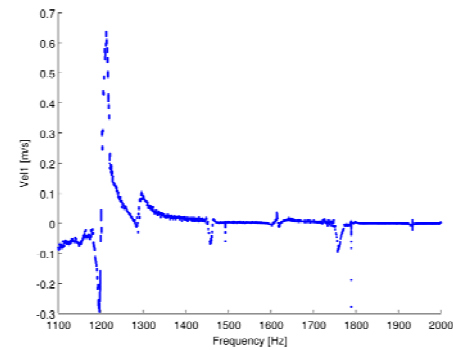
quency step. In particular, in the bifurcation diagram of the Poincaré maps (Figure 17m) there are at least two regions with non stationary response, while for the other run (1Hz frequency step, Figure 17l) there was only a narrow non stationary band close to 1200Hz. For 0.1Hz frequency step, the non-stationary response bands are 1170-1183Hz and 1198-1210Hz. Looking at Figure 17n it can be clearly noticed that the lowest non-stationary region (1170-1183Hz) is split into two sub-regions, since at 1175Hz in the downwards run the complexity of the system increases, i.e. the vibrational energy spreads over the whole spectrum.



(a) Bifurcation diagram of the Poincaré maps at 0.1V downwards (b) Waterfall diagram at 0.1V downwards

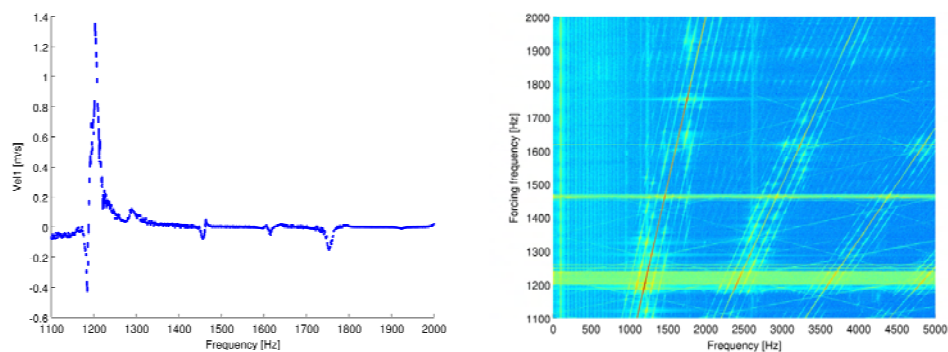


(c) Bifurcation diagram of the Poincaré maps at 0.3V downwards (d) Waterfall diagram at 0.3V downwards

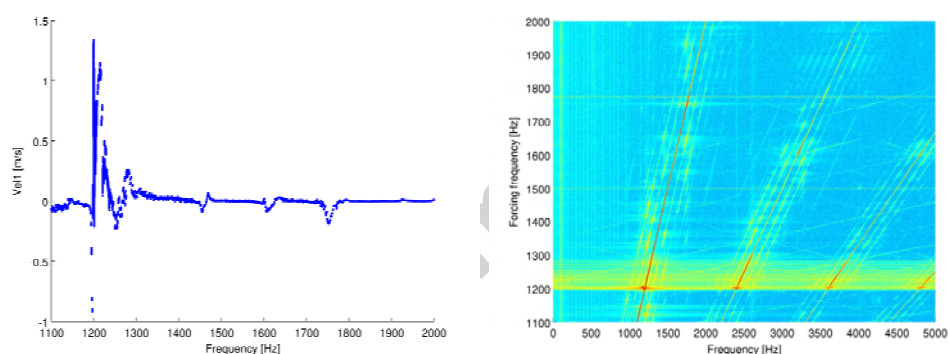


(e) Bifurcation diagram of the Poincaré maps at 0.5V downwards (f) Waterfall diagram at 0.5V downwards

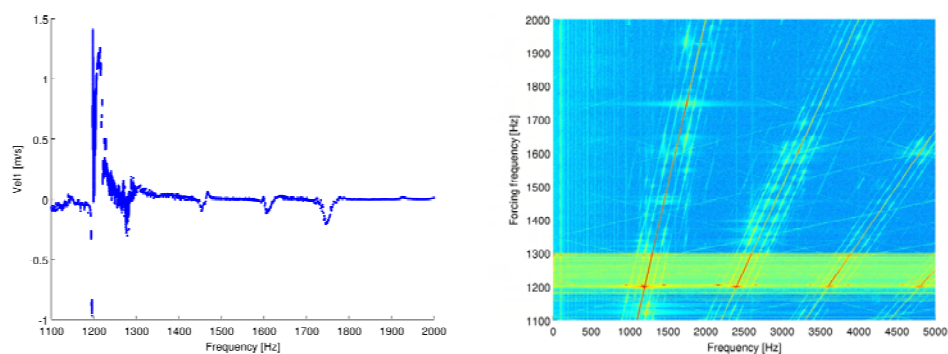
Figure 17: Bifurcation diagram of the Poincaré maps and waterfall diagram of power spectrum - Lateral velocity - 250N preload (continued on next page)



(g) Bifurcation diagram of the Poincaré maps at 0.7V downwards (h) Waterfall diagram at 0.7V downwards

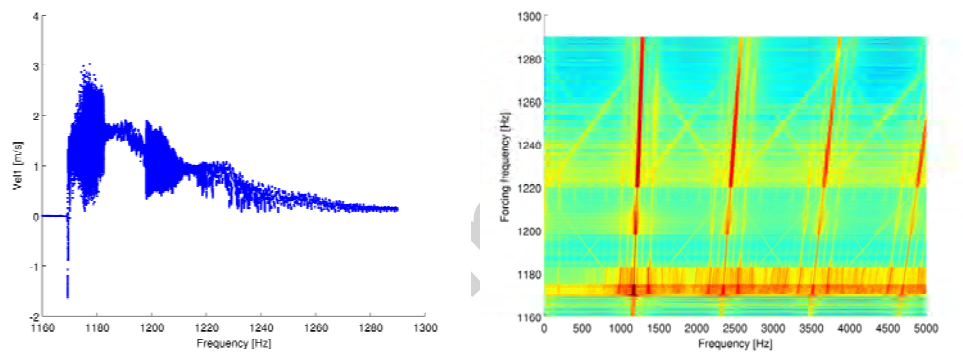


(i) Bifurcation diagram of the Poincaré maps at 0.9V downwards (j) Waterfall diagram at 0.9V downwards



(k) Bifurcation diagram of the Poincaré maps at 1.0V downwards (l) Waterfall diagram at 1.0V downwards

Figure 17: Bifurcation diagram of the Poincaré maps and waterfall diagram of power spectrum - Lateral velocity - 250N preload (continued from previous page)



(m) Bifurcation diagram of the Poincaré maps at 1.0V downwards run 2
(n) Waterfall diagram of power spectrum - Lateral velocity - 250N preload (continued from previous page)

Figure 17: Bifurcation diagram of the Poincaré maps and waterfall diagram of power spectrum - Lateral velocity - 250N preload (continued from previous page)

7.1. 0.9V Downwards

A detailed analysis of the dynamic scenario occurring in the fast run (1Hz step) at 0.9V is shown in Figures 18 and 19. At 1196Hz the response is periodic, as confirmed by the Poincaré map, which consists of a single point. At 1200Hz, the Poincaré map is closed line both in (base acceleration, lateral vibration) and in (dynamic axial load, lateral vibration) plane, this confirms that the non-stationarity seen in the corresponding bifurcation diagram of the Poincaré maps (Figure 17i) is a quasiperiodic response. At 1208Hz the response is again 1T periodic.

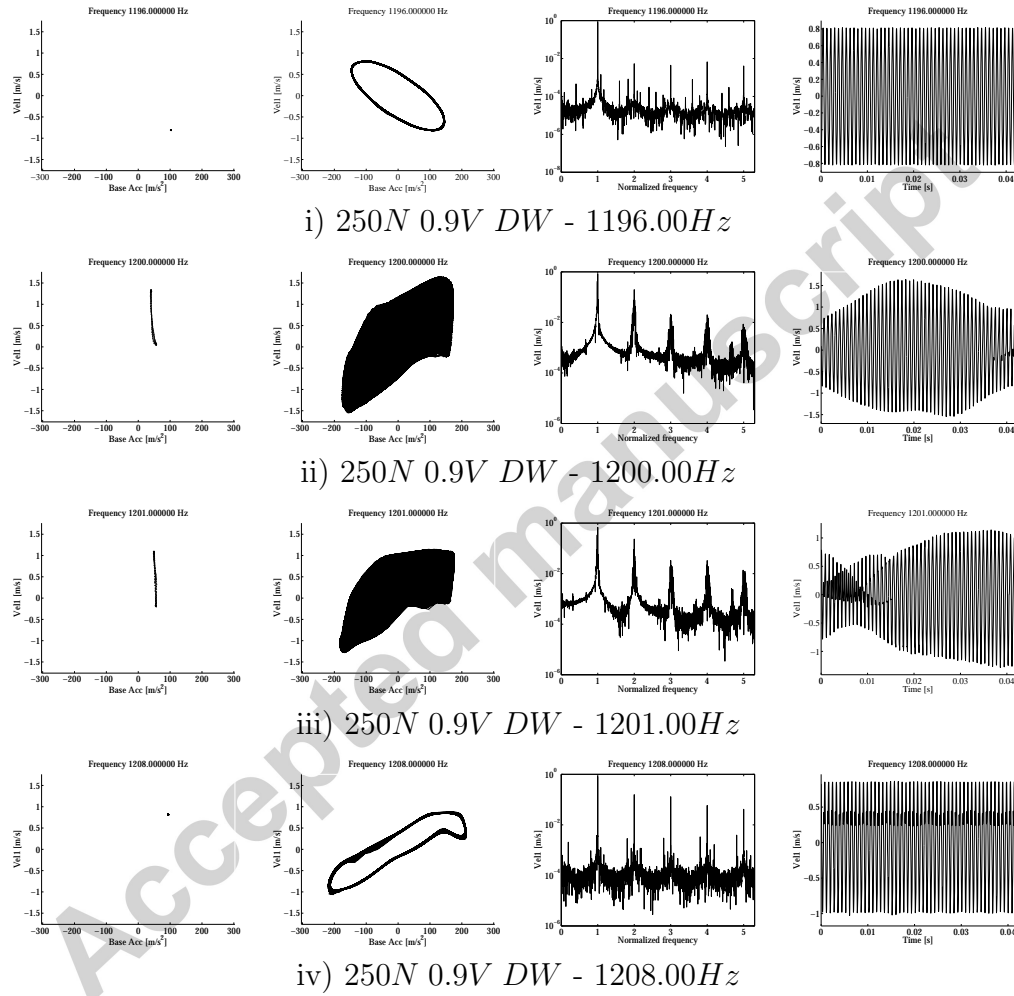


Figure 18: Base acceleration - Lateral velocity: Poincaré maps, phase portraits, spectra and time histories at 250N 0.9V downwards

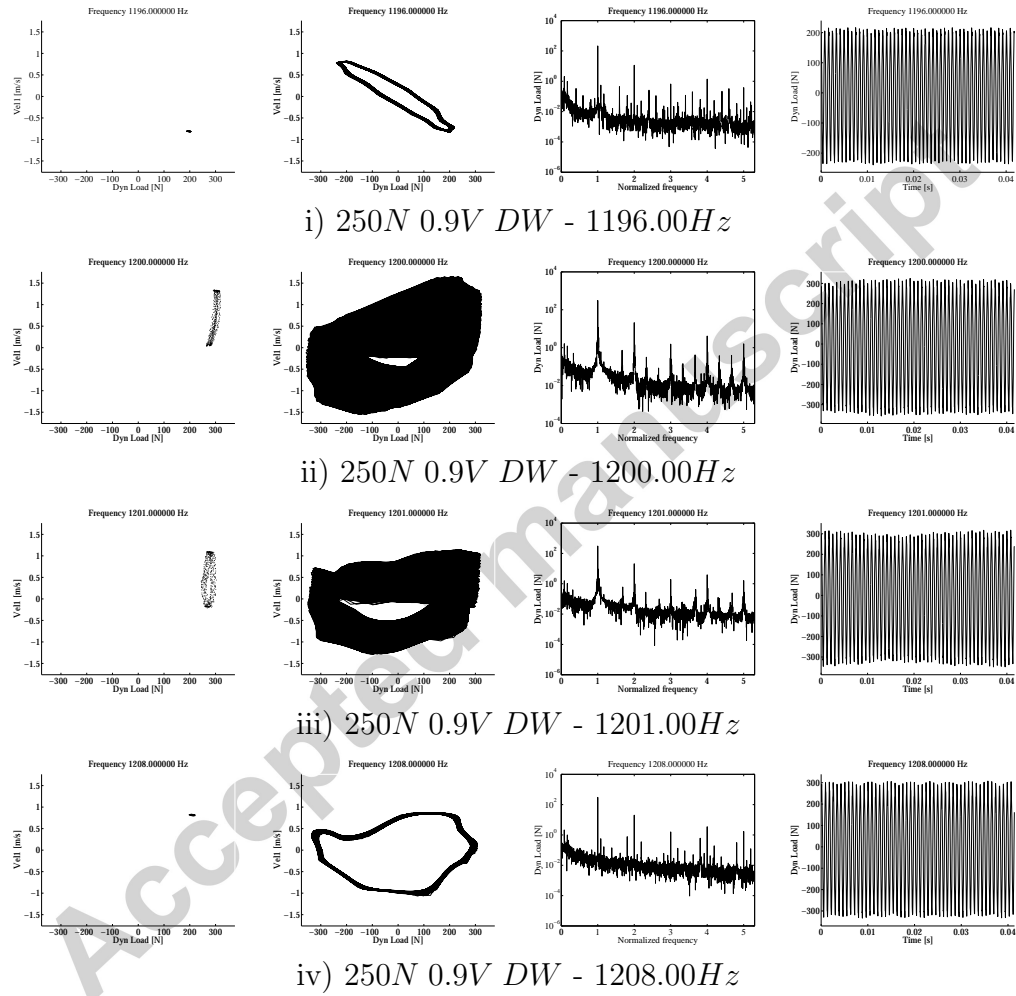


Figure 19: Dynamic load - Lateral velocity: Poincaré maps, phase portraits, spectra and time histories at 250N 0.9V downwards

7.2. 1.0V Downwards - run 2

The following test case has been performed with a frequency step of 0.1Hz, ten times less than the previous. The measured response in the slower step sine (0.1 Hz) is significantly different with respect to the fast test (1Hz), as observed in the amplitude-frequency diagrams, see Figure 16. In run 2, the finer frequency step allows following less stable solutions, and larger instability regions are found. It is obvious that, reducing the frequency step reduces the perturbation when the frequency is varied, smaller is the step, better a bifurcation is followed. On the other hand a finer frequency steps increases both testing time and amount of data, the latter one is limited by the hardware capabilities.

At 1169.50Hz the response is quasiperiodic, as confirmed by the Poincaré map both in the (base acceleration, lateral vibration) and in (dynamic axial load, lateral vibration) plane, see Figures 20 and 21. At 1182.50Hz the system presents a chaotic response, with a fractal Poincaré map. At higher frequency, 1182.70 the response is stationary again, as confirmed by the Poincaré map and the phase portrait.

The second non stationary region starts at 1198Hz with a quasiperiodic response, clearly visible in the Poincaré maps (Figures 20 and 21). Note that on the (dynamic axial load, lateral vibration) plane the response can look similar to a chaotic attractor, but it is more likely to be a closed curve, with a non negligible dispersion, which is due to a larger uncertainty in the dynamic load with respect to the base acceleration measurement.

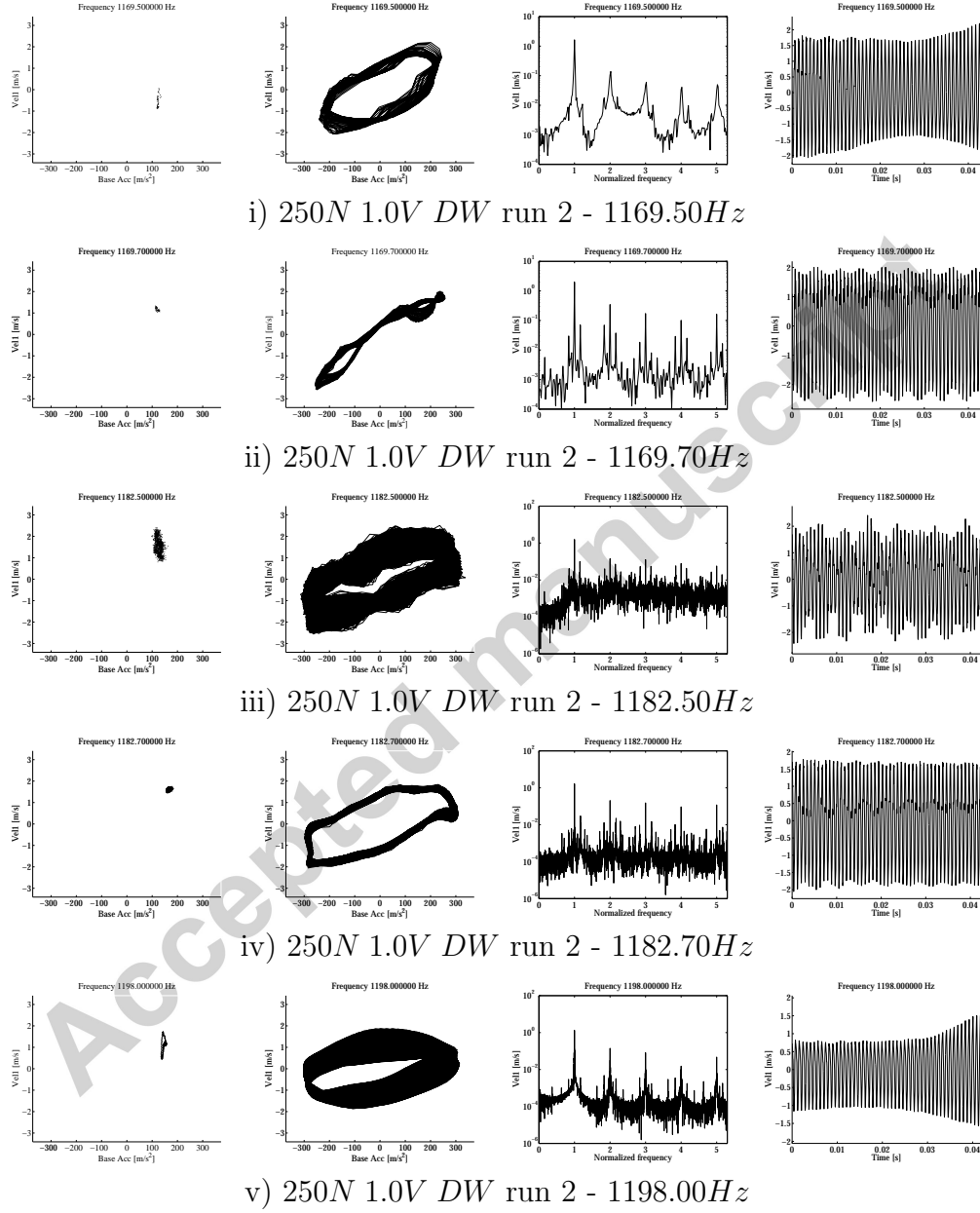


Figure 20: Base acceleration - Lateral velocity: Poincaré maps, phase portraits, spectra and time histories at 250N 1.0V run 2 downwards

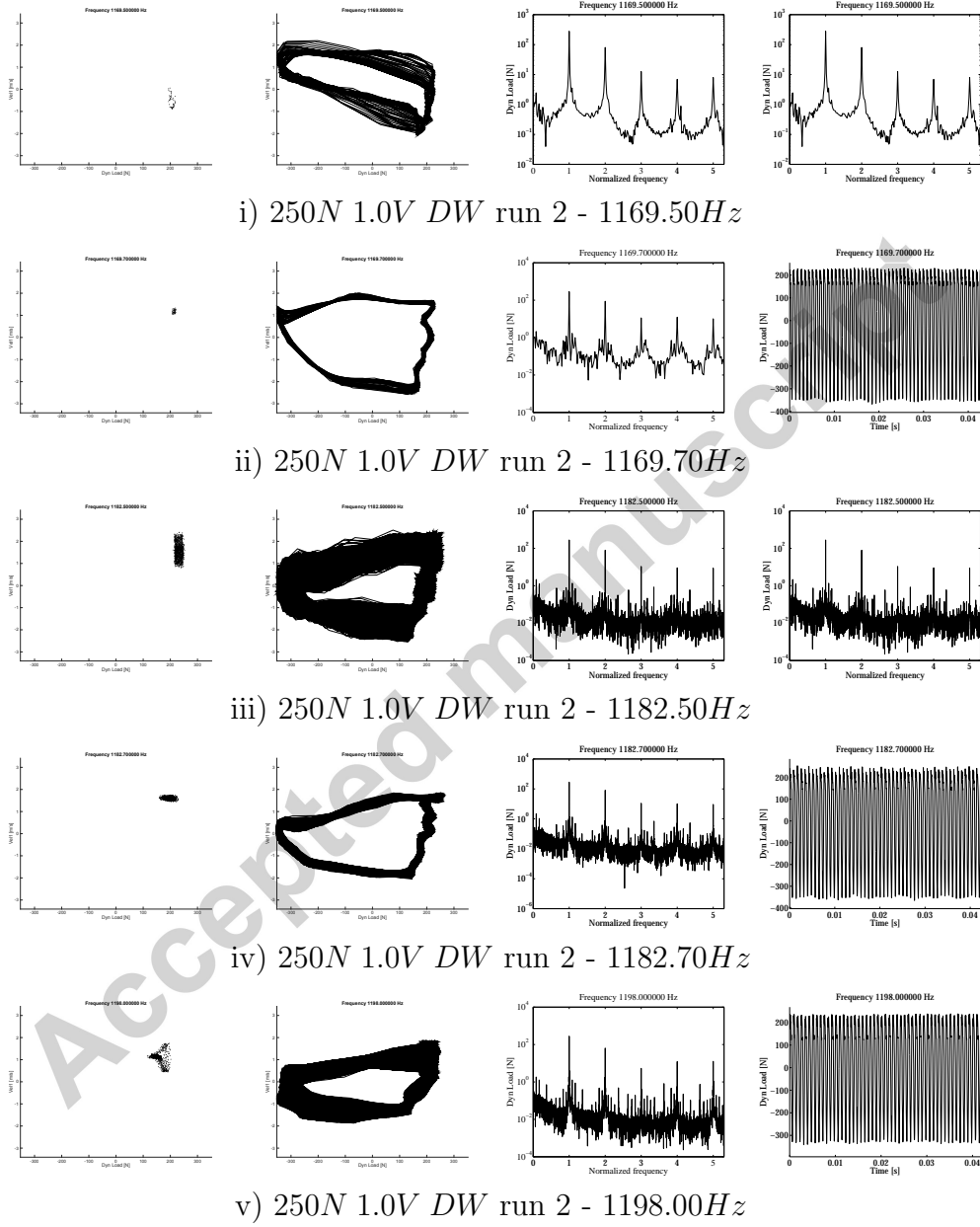


Figure 21: Dynamic load - Lateral velocity: Poincaré maps, phase portraits, spectra and time histories at 250N 1.0V run 2 downwards

8. Conclusions

The nonlinear dynamics of pre-compressed circular cylindrical shells have been investigated by experiments. A new setup has been developed in order to apply both static and dynamic axial load to the shell.

The linear dynamics of a pre-compressed shell has been studied by using a micro-hammer impact testing. These investigations show that there is a very limited effect of the pre-load on the natural frequency, as suggested by the theory. This preliminary investigation is very important in validating the experimental setup, ensuring that the device introduced for applying the preload and the clamping of the shell performs in the desired way.

The tests performed with a sinusoidal axial excitation clarify the role of the preload in enlarging the instability regions. These tests have been performed using an open loop strategy with a novel technique for providing a very smooth sine step excitation, i.e., the signal is a sine step joined with sine sweep connections. This procedure, which is able to provide a continuous signal during the whole duration of a test performed at varying frequency, allows for following dynamic states with a limited stability, and to observe strongly subharmonic responses by experiments.

Among the non-linear phenomena observed during the experiments, it is worthwhile noting a quasiperiodic response at 100N preload which collapse into a strongly subharmonic attractor (20T) and then becomes quasiperiodic again within a 2Hz frequency range. The occurrence of this subharmonic solution can be explained by the conjecture that the frequency of the sidebands is variable and can have a rational ratio with respect to the fundamental excitation frequency.

Another important feature pointed out by the experiments is the coexistence of more than one stable states, when the shell is pre-loaded and excited with a moderately large sinusoidal excitation. The tests show that the dynamic scenario is completely different if the frequency step is reduced from 1Hz to 0.1Hz, with larger instability regions and a completely different amplitude-frequency diagram. It is to point out that 1 or 0.1Hz frequency step are not right or wrong in principle, but represent different excitations that lead to different responses and scenarios

- [1] A. W. Leissa, Vibration of shells, NASA SP-288, Scientific and Technical Information Office, National Aeronautics and Space Administration; Washington, DC, 1973.

- [2] T. Von Kármán, H. Tsien, The buckling of thin cylindrical shells under axial compression, *Journal of the Aeronautical Sciences* 8 (8) (1941) 303–312.
- [3] J. Teng, Buckling of thin shells: Recent advances and trends., *Applied Mechanics Reviews* 49 (4) (1996) 263–274.
- [4] V. D. Kubenko, P. S. Koval'chuk, T. S. Krasnopol'skaya, Nonlinear interaction of the flexural modes of vibration of cylindrical shells, *Nauk. Dumka*, 1984.
- [5] P. K. V.D. Kubenko, Nonlinear problems of the vibration of thin shells (review)., *International Applied Mechanics* 34 (1998) 703–728.
- [6] M. P. M. Amabili, Review of studies on geometrically nonlinear vibrations and dynamics of circular cylindrical shells and panels, with and without fluid-structure interaction., *Applied Mechanics Reviews* 56 (2003) 349–381.
- [7] V. D. Kubenko, P. S. Koval'chuk, Influence of initial geometric imperfections on the vibrations and dynamic stability of elastic shells, *International Applied Mechanics* 40 (8) (2004) 847–877.
- [8] F. Alijani, M. Amabili, Non-linear vibrations of shells: A literature review from 2003 to 2013, *International Journal of Non-Linear Mechanics* 58 (0) (2014) 233–257. doi:<http://dx.doi.org/10.1016/j.ijnonlinmec.2013.09.012>.
- [9] R. Fey, N. Mallon, C. Kraaij, H. Nijmeijer, Dynamic stability of two harmonically excited thin-walled structures carrying a top mass, in: *Proceedings of the 11th European Conference on Spacecraft Structures, Materials and Mechanical Testing*, 2009, pp. 1–7.
- [10] A. Vijayaraghavan, R. M. Evan-Iwanowski, Parametric instability of circular cylindrical shells, *Journal of Applied Mechanics* 34 (4) (1967) 985–990. doi:10.1115/1.3607867.
- [11] M. A. Souza, Coupled dynamic instability of thin-walled structural systems, *Thin-Walled Structures* 20 (1994) 139–149.

- [12] A. Sofiyev, N. Kuruoglu, Buckling and vibration of shear deformable functionally graded orthotropic cylindrical shells under external pressures, *Thin-Walled Structures* 78 (2014) 121–130.
- [13] M. Strozzi, F. Pellicano, Nonlinear vibrations of functionally graded cylindrical shells, *Thin-Walled Structures* 67 (0) (2013) 63–77. doi:<http://dx.doi.org/10.1016/j.tws.2013.01.009>.
- [14] M. Ray, J. Shivakumar, Active constrained layer damping of geometrically nonlinear transient vibrations of composite plates using piezoelectric fiber-reinforced composite, *Thin-Walled Structures* 47 (2009) 178–189.
- [15] A. Zippo, G. Ferrari, M. Amabili, M. Barbieri, F. Pellicano, Active vibration control of a composite sandwich plate, *Composite Structures* 128 (2015) 100–114. doi:<http://dx.doi.org/10.1016/j.compstruct.2015.03.037>.
- [16] A. Jafari, S. Khalili, M. Tavakolian, Nonlinear vibration of functionally graded cylindrical shells embedded with a piezoelectric layer, *Thin-Walled Structures* 79 (8-15).
- [17] M. Amabili, *Nonlinear Vibrations and Stability of Shells and Plates*, Cambridge University Press, 2008.
URL <http://dx.doi.org/10.1017/CB09780511619694>
- [18] P. B. Gonçalves, Z. J. Del Prado, Nonlinear oscillations and stability of parametrically excited cylindrical shells, *Meccanica* 37 (2002) 569–597.
URL <http://dx.doi.org/10.1023/A:1020972109600>
- [19] F. Pellicano, K. Avramov, Linear and nonlinear dynamics of a circular cylindrical shell connected to a rigid disk, *Communications in Nonlinear Science and Numerical Simulation* 12 (4) (2007) 496–518. doi:<http://dx.doi.org/10.1016/j.cnsns.2005.04.004>.
- [20] V. Kubenko, P. Koval’chuk, Experimental studies of the vibrations and dynamic stability of laminated composite shells, *International Applied Mechanics* 45 (2009) 514–533.
- [21] S. Patel, P. Datta, A. Sheikh, Buckling and dynamic instability analysis of stiffened shell panels, *Thin-Walled Structures* 44 (2006) 321–333.

- [22] F. Bakhtiari-Nejad, S. M. Mousavi Bideleh, Nonlinear free vibration analysis of prestressed circular cylindrical shells on the winkler/pasternak foundation, *Thin-Walled Structures* 53 (2012) 26–39.
- [23] F. Pellicano, Dynamic instability of circular cylindrical shells subject to base excitation, *Civil-Comp Proceedings* 99.
- [24] F. Pellicano, M. Barbieri, A. Zippo, M. Strozzi, Experiments on shells under base excitation, *Journal of Sound and Vibration* 369 (2016) 209–227. doi:<http://dx.doi.org/10.1016/j.jsv.2015.12.033>.
- [25] F. Pellicano, Vibrations of circular cylindrical shells: theory and experiments, *Journal of Sound and Vibration* 303 (2007) 154–170.
- [26] F. Pellicano, Dynamic instability of a circular cylindrical shell carrying a top mass under base excitation: Experiments and theory, *International Journal of Solids and Structures* 48 (2011) 408–427.
- [27] F. Pellicano, M. Barbieri, Complex dynamics of circular cylindrical shells, *International Journal of Non-Linear Mechanics* 65 (2014) 196–212. doi:<http://dx.doi.org/10.1016/j.ijnonlinmec.2014.05.006>.
- [28] W. Soedel, *Vibrations of Shells and Plates*, Marcel Dekker Inc., New York, 1993.
- [29] A. Zippo, Nonlinear dynamics and active vibration control of thin walled structures, Ph.D. thesis, University of Modena and Reggio Emilia (2014).